Received: 9 April 2025 | Accepted: 1 August 2025

DOI: 10.1002/bmm2.70031

RESEARCH ARTICLE

BMEMat WILEY

Deciphering the catalytic and pharmacological mechanisms of Coptis chinensis herbzymes to renovate intestinal microenvironment for colitis alleviation

Zhichao Deng[1] | **Can Li**[2] | **Yujie Zhang**[1] | **Yuanyuan Zhu**[1] | **Chenxi Xu**[1] | **Bowen Gao**[1] | **Mingxin Zhang**[3] | **Martina H. Stenzel**[4] | **Kelong Fan**[5,6] | **Mingzhen Zhang**[1] | **Yanyan Jiang**[2]

[1]School of Basic Medical Sciences, Xi'an Jiaotong University, Xi'an, China

[2]Key Laboratory for Liquid-Solid Structural Evolution & Processing of Materials (Ministry of Education), School of Materials Science and Engineering, Shandong University, Jinan, China

[3]Department of Gastroenterology, The First Affiliated Hospital of Xi'an Medical University, Xi'an, China

[4]School of Chemistry, University of New South Wales (UNSW), Sydney, Australia

[5]CAS Engineering Laboratory for Nanozyme, Key Laboratory of Biomacromolecules (CAS), CAS Center for Excellence in Biomacromolecules, Institute of Biophysics, Chinese Academy of Sciences, Beijing, China

[6]Nanozyme Laboratory in Zhongyuan, Henan Academy of Innovations in Medical Science, Zhengzhou, China

Correspondence
Kelong Fan, Mingzhen Zhang and Yanyan Jiang.
Email: fankelong@ibp.ac.cn, mzhang21@xjtu.edu.cn and yanyan.jiang@sdu.edu.cn

Funding information
National Natural Science Foundation of China, Grant/Award Numbers: 82472127, 52101287, 82300598; Fundamental Research Funds for the Central Universities, Grant/Award Number: xtr052023008; Young Talent Support Plan of Xi'an an Jiaotong University, Grant/Award Number: YX6J001

Abstract

Leveraging the traditional medicinal properties of the intestinal meridian herb *Coptis chinensis* (CC), CC carbon dots nanozymes (CCzymes) are developed for the treatment of ulcerative colitis (UC). The CC precursors provide functional fragments and oxygenated functional groups that endow CCzymes with pharmacological activity and potent scavenging ability of free radicals. Targeting UC, CCzymes can effectively promote the restoration of the intestinal microenvironment. CCzymes inhibit the secretion of pro-inflammatory cytokines downstream of the MAPK and PI3K-Akt signaling pathways by suppressing the expression of the gene encoding the receptor tyrosine kinase protein (Kit). At the same time, CCzymes inhibited the HIF-1 and JAK-STAT signaling pathways, which in turn inhibited M1-type polarization of macrophages. In addition, CCzymes selectively inhibit pathogenic bacteria while promoting the growth of beneficial microbiota, thus achieving a balanced gut microbiota. Importantly, CCzymes also increased the levels of bile acids and indole derivatives, thereby contributing to the restoration of intestinal barrier integrity. This study provides a novel approach to harness the therapeutic potential of herbal nano-enzymes, offering a powerful strategy for treating

Zhichao Deng and Can Li contributed equally to this work.

This is an open access article under the terms of the Creative Commons Attribution License, which permits use, distribution and reproduction in any medium, provided the original work is properly cited.

© 2025 The Author(s). *BMEMat* published by John Wiley & Sons Australia, Ltd on behalf of Shandong University.

inflammatory diseases through targeted antioxidant therapy. Targeting UC, CCzymes can be effective in treating inflammatory diseases.

KEYWORDS
carbon dots, Coptis chinensis, herbzymes, ulcerative colitis

1 | INTRODUCTION

Ulcerative colitis (UC) is a type of chronic disease caused by intestinal imbalances, involving the intestinal immune system and microbial interactions.[1] Specifically, due to impaired intestinal barrier, gut microbiota and metabolic dysregulation, and reactive oxygen species (ROS) burst, patients directly face chronic relapsing intestinal inflammation, mucosal ulcers, intestinal dysfunction, and systemic complications.[2] Therefore, this disease has a serious impact on the health of millions of people around the world, increasing the risk of colorectal cancer (CRC).[3] Currently, aminosalicylates and glucocorticoids are the primary medications utilized in the treatment of UC. However, these drugs are associated with significant side effects and varying levels of efficacy. In response to these limitations, novel nanomaterials with inherent anti-inflammatory and antioxidant properties have been developed to improve the treatment outcomes of UC.[4] Nevertheless, the potential biotoxicity and effectiveness of these nanomaterials, as well as their mechanisms underlying the efficacy, remain inadequately researched, thereby impeding their broader application in clinical settings. Consequently, there is a pressing need to explore and develop new pharmaceutical nanomaterials that are both safe and effective in the management and treatment of UC.

Chinese herbal medicine, recognized for its high medicinal activity, low cost, and non-toxicity, has garnered increasing interest. For instance, Phellodendron Bark,[5] Coptis chinensis (CC),[6] and Rhizoma Atractylodis Macrocephalae[7] have shown significant effects in treating UC. Specifically, berberine (BBR) in CC has been found to regulate intestinal immune cells, thereby alleviating mucosal inflammation.[8] Studies also have shown that BBR is negatively correlated with inflammation-related pathways and can significantly inhibit the activity of inflammation-related pathways such as the TNF signaling pathway and the JAK-STAT signaling pathway. Meanwhile, BBR can significantly adjust the microbial community structure, increasing the relative abundance of Firmicutes and reducing the content of Proteobacteria.[9] Moreover, the polysaccharides in CC play a crucial role in modulating the gut microbiota and immune response.[10] These therapeutic properties of CC contribute to mitigating oxidative stress, enhancing the colonic epithelial barrier, and effectively managing UC.[11] Despite these benefits, the poor water-solubility of the active components in Chinese medicine often results in limited absorption rates and therapeutic outcomes.

Carbon dots (CDs), featuring sizes smaller than 10 nm, are photoluminescent nanomaterials widely employed in biosensing, disease diagnosis, and treatment due to their excellent water solubility and biosafety.[12] The performance of CDs is significantly influenced by the nature of the carbon precursor, as incomplete carbonization during their formation may lead to the retention and incorporation of functional groups from the precursor, thereby inheriting its biological activity.[13] For instance, Ginger-derived CDs have been shown to block the TLR4/NF-κB phosphorylation pathway, effectively suppressing the overexpression of associated inflammatory mediators and promoting wound healing.[14] CDs prepared using the anti-inflammatory herbs Scutellaria barbata and Herba Hedyotis diffusae as precursors exhibit efficient radical scavenging properties.[15] Besides forming an internal carbon core, CDs also boast a polymer shell abundant in functional groups on their surface.[16] This feature grants them excellent water solubility and potentially a wider range of physicochemical properties, including enzyme-like activity.[17, 18] Numerous studies have successfully developed enzyme-mimicking CDs, such as such as peroxidase-like, catalase (CAT),[19] and superoxide dismutase (SOD) mimics. CDs nanozymes can effectively regulate ROS levels with higher stability and lower cost compared to natural enzymes.[20, 21] Therefore, by utilizing Chinese medicinal herbs as precursors to produce CDs, the solubility and bioavailability of the active ingredients can be enhanced. In addition, this approach also enables the creation of highly efficient antioxidant nanozymes with free radical scavenging abilities. These advancements offer valuable insights into leveraging Chinese herbal medicine in the biomedical field.

In this study, we have proposed the fabrication of CDs nanozymes utilizing herbal medicines as precursor materials, referred to as herbzymes. We used CC as a precursor and constructed CDs-based nanozymes (CCzymes) with antioxidant enzyme activity for the treatment of UC through a facile one-step hydrothermal method. CCzymes

retain the effective functional group fragments present in the active ingredients of CC and subsequently inherit the pharmacological activities of the precursors. The abundance of carbonyl groups conjugated to the π-system on the surface of CCzymes facilitates charge transfer at the active site, promoting enzymatic activities, such as SOD-like and •OH scavenging. Due to these, CCzymes exhibit superior antioxidant enzyme activities compared to CC extract. The utilization of CCzymes allows for the efficient facilitation of UC therapy by effectively renovating the intestinal microenvironment. Specifically, in the cellular environment, CCzymes demonstrate a robust anti-inflammatory through the inhibition of inflammatory signaling pathways by downregulating the expression of the receptor tyrosine kinase (Kit) and the modulation of macrophage polarization, leading to a reduction in inflammation. Additionally, CCzymes selectively target pathogenic bacteria while increasing beneficial bacteria levels, thereby modulating the gut microbiota. Notably, by promoting the production of bile acids and indole derivatives, CCzymes can restore damaged intestinal barrier function (Figure 1). In conclusion, CCzymes exhibit potent therapeutic effects in acute and chronic UC treatment, marking a promising avenue for managing inflammatory diseases using novel herbzymes with robust antioxidant properties derived from herbs.

2 | RESULTS

2.1 | Synthesis and characterization of CCzymes

The CCzymes were derived from CC using a straightforward hydrothermal process, as illustrated in Figure 2a. The results of transmission electron microscopy (TEM) and atomic force microscopy (AFM) indicated that the CCzymes exhibited an average size of approximately 2.5 nm, with a tightly clustered structure (Figure 2b). DLS characterization determined the hydrodynamic diameter of CCzymes and revealed a surface potential of −14.27 mV (Figure S1 and S2). Additionally, the average height of the CCzymes was determined to be approximately 2.1 nm, as shown in Figure 2c. These findings indicate that the as-prepared CCzymes possess a high degree of uniformity in spherical shape, with a size advantage that facilitates efficient penetration of biological barriers.[22] Additionally, the CCzymes demonstrated good crystallinity, as evidenced by distinct lattice fringes measuring 0.21 nm corresponding to the (100) planes of graphite carbon.[23, 24] The X-ray diffraction (XRD) pattern revealed an amorphous broad peak at 22.4° indicative of graphite carbon (Figure S3). These results collectively support the successful synthesis of CCzymes with CDs structure. The Raman spectrum depicted in Figure 2d exhibited a peak at 1350 cm^{-1} attributed to the D band of the graphitic ordered structure, as well as a peak at 1580 cm^{-1} linked to the G band of the graphitic disordered structure, with an intensity ratio of I_D/I_G = 1.05. It is suggested that the CCzymes possess a graphitic structure with a significant number of defects, which may endow their catalytic performance as enzymes.[25]

Intrinsic fluorescence emission is a characteristic feature of CDs, as observed in CCzymes. The UV-visible absorption spectrum of CCzymes displayed absorption peaks at 277 and 340 nm, indicative of π-π* transitions and n-π* transitions, respectively (Figure 2e). The occurrence of the π-π* transition in CCzymes can be attributed to the presence of sp^2 hybridized domains in the carbon core, leading to the excitation of π-bonded electrons from π-orbitals to π*-orbitals upon absorption of UV light. On the other hand, the n-π* transition is a result of the existence of oxygen-containing functional groups such as hydroxyl (-OH), carbonyl (C=O), and carboxyl (-COOH) in CCzymes, causing non-bonding electrons (n-electrons) to be excited to π*-orbitals upon absorption of photons. The excitation of electrons through both π-π* and n-π* transitions contributes to the exceptional optical properties of CCzymes.[16, 26] The excitation-emission maximum spectra of CCzymes, in conjunction with both 2D and 3D fluorescence spectra (Figure 2f), exhibited an excitation range from 378 to 390 nm, with a narrow emission peak between 477 and 510 nm. The optimal excitation wavelength was determined to be 384 nm, with an optimal emission wavelength of 492 nm, resulting in a fluorescence lifetime of 3.84 ns (Figure 2g) and a fluorescence quantum yield of 4.1% (Figure S4). Given these favorable optical characteristics, the potential utility of CCzymes in fluorescent anti-counterfeiting applications was subsequently investigated. The QR code, printed with an aqueous solution of CCzymes, exhibited blue fluorescence under UV light exposure, thereby enabling successful scanning and revealing the concealed pattern information (Figure S5). The green synthesis, low cost, and remarkable chemical stability of CCzymes offer the potential for advancing the field of optical anti-counterfeiting within the printing industry, as well as expanding their applications in biological research.[27]

Subsequent investigation into the structural information of CCzymes was performed using Fourier-transform infrared (FTIR) spectroscopy and X-ray photoelectron spectroscopy (XPS). In the FTIR spectrum, both the CC extract and CCzymes exhibited an absorption peak at 3404 cm^{-1} corresponding to -NH/OH stretching, and a

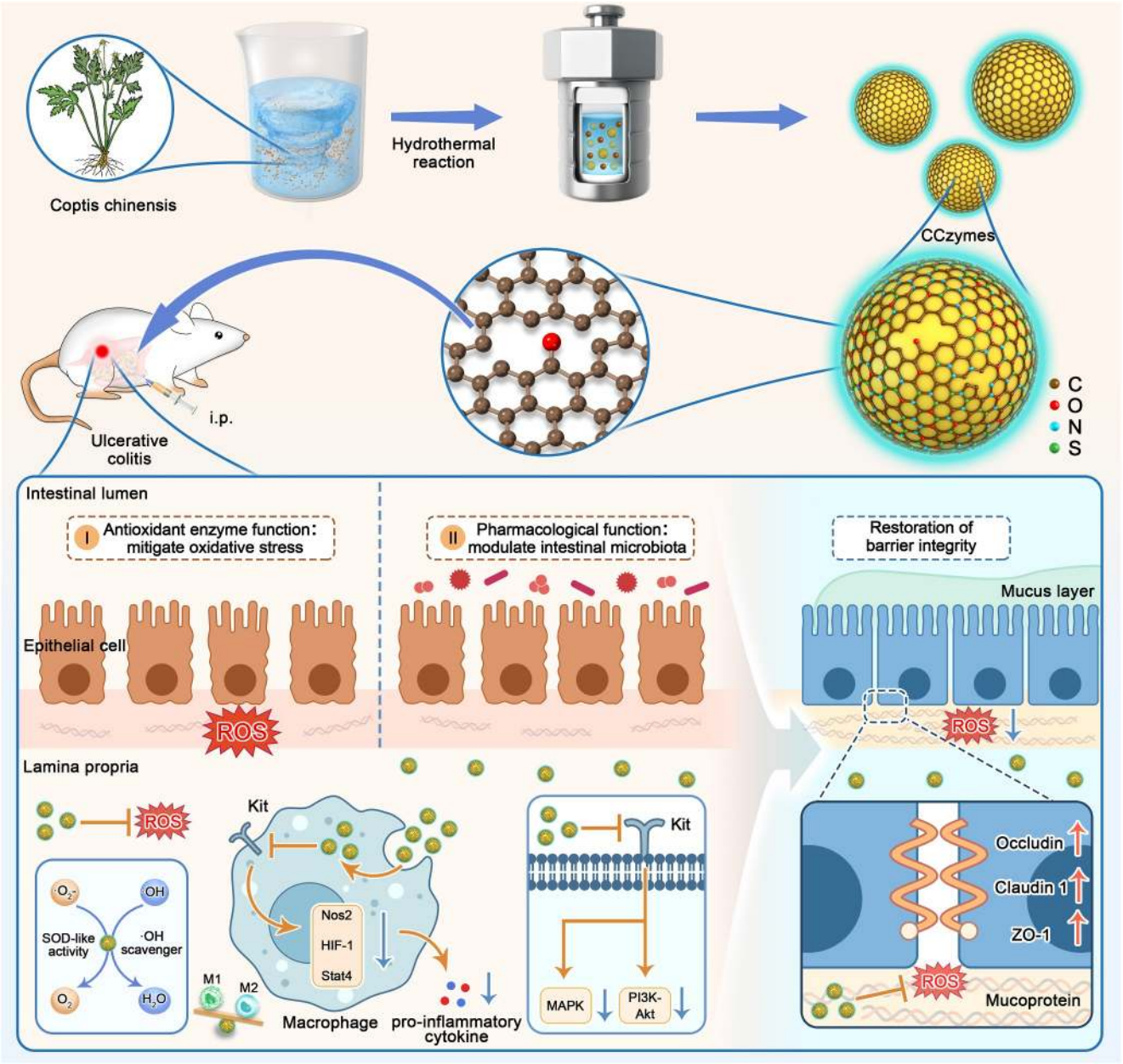

FIGURE 1 The diagram depicts the process of synthesizing CCzymes and their role in mitigating UC through various mechanisms. CCzymes were synthesized through a one-step hydrothermal process utilizing CC as the primary source material. As herbzymes, CCzymes exhibit dual functionality, encompassing antioxidant enzyme activity as well as the pharmacological attributes inherent to CC. In the context of UC treatment, CCzymes demonstrate the capacity to mitigate oxidative stress within inflamed regions by virtue of their antioxidant enzyme activity, while also leveraging the intrinsic characteristics of CC to modulate macrophage polarization and intestinal microbiota. Ultimately, the application of CCzymes facilitates the restoration of the intestinal epithelial barrier in UC, thereby contributing to the therapeutic management of this condition. CC, Coptis chinensis; UC, ulcerative colitis.

peak at 2954 cm^{-1} associated with C-H stretching, along with a continuous -CH_2 wagging vibration at 720 cm^{-1}(Figure 2h).[28] In comparison to the CC extract, the peaks corresponding to C=O and C−O functional groups at 1630 and 1091 cm^{-1} in the CCzymes were notably intensified, indicating a greater abundance of oxygen-containing functional groups.[29] The enhanced water solubility of CCzymes can be attributed to the substantial presence of hydrophilic functional groups (-OH/-NH and C-O) on their surface.[15] The XPS survey spectrum in Figure 2l revealed the presence of carbon (C), oxygen (O), and nitrogen (N) in the CC extract, with atomic percentages of 79.39%, 17.54%, and 3.08%, respectively. In contrast, CCzymes exhibited a higher oxygen content, with atomic percentages of 69.86% for C, 21.67% for O, and 3.46% for N. The high-resolution N 1s spectra for both samples were

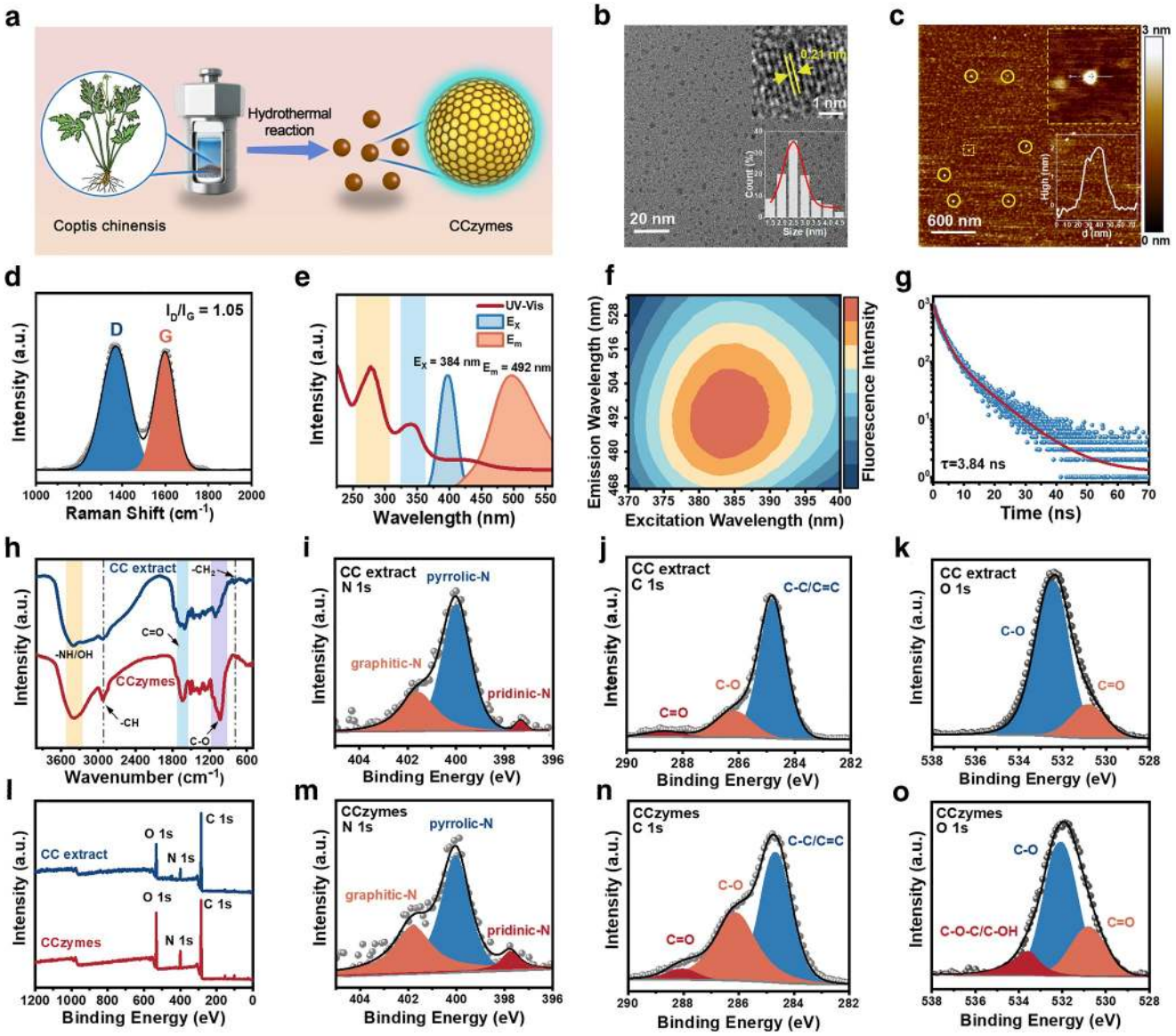

FIGURE 2 Synthesis and characterization of CCzymes. (a) Schematic of the fabrication of CCzymes. (b) TEM image, HR-TEM image, and histogram of the size distribution of CCzymes. (c) atomic force microscopy image, histogram of the height distribution of CCzymes. (d) Raman spectrum and (e) UV–Vis spectra, 2D fluorescence spectroscopy of CCzymes. (f) 3D fluorescence spectroscopy and (g) PL-decay curves of CCzymes. (h) FT-IR spectra of CCzymes and CC extract. (i–k) High-resolution XPS spectra of C 1s, O 1s, and N 1s for CC extract. (l) XPS survey spectra of CCzymes and CC extract. (m–o) High-resolution XPS spectra of C 1s, O 1s, and N 1s for CCzymes. CC, Coptis chinensis; TEM, transmission electron microscopy; XPS, X-ray photoelectron spectroscopy.

analyzed, showing three distinct components corresponding to graphitic-N, pyrrolic-N, and pyridinic-N (Figure 2i,m).

Furthermore, Figure 2j,n displays the high-resolution C 1s spectra of the CC extract and CCzymes, which consist of three peaks corresponding to C−C/C=C at 284.8 eV, C−O at 285.7 eV, and C=O at 288.2 eV. The high-resolution O 1s spectra comparison showed that the deconvoluted CCzymes display a higher peak for C=O at 530.7 eV compared to the extract, consistent with the C 1s spectra (Figure 2k,o).[28] Significantly, in addition to the prominent peak at 532.0 eV corresponding to C-O bonds, CCzymes exhibited a peak at 533.5 eV, which might be attributed to C-O-C and C-OH structures.[30] The identification of the C-O-C moiety prompted further analysis of the structural characteristics of CCzymes. Therefore, the ^{1}H Nuclear Magnetic Resonance (NMR) spectra of the extract, CCzymes, and berberine were compared (Figure S6). Signals corresponding to hydrogens at the a, b, and c positions of the berberine structure at chemical shifts of 5.79, 6.67, and 7.18 ppm, the cyclic ether bonds (C-O-C structure) playing a significant role in the

biological activity of berberine, were also observed in CCzymes. In contrast, the CC extract did not exhibit this trait. It is implied that the functional groups of berberine are successfully incorporated into the structure of CDs during the carbonization process, potentially retaining the characteristics of the active components from the precursor. Furthermore, CCzymes exhibited a distinct peak at 4.75 ppm, a characteristic peak often assigned to oxygen-containing functional groups.[22] These findings suggest that, in line with the FTIR and XPS analyses, the CCzymes produced through carbonization demonstrate an increased presence of oxygen functional groups, particularly carbonyl groups, which contribute to their antioxidant activities.

2.2 | Deciphering the catalytic mechanism of CCzymes

Subsequently, the antioxidant enzyme activity of CCzymes was examined. Hydroxyl radicals (•OH) are prevalent harmful free radicals that induce oxidative damage to cells. To assess the ability of CCzymes to capture and neutralize •OH, the TMB colorimetric assay was employed using 3,3′,5,5′-tetramethylbenzidine (TMB) as a probe. The Fenton reaction was employed to generate •OH, which oxidized TMB to oxTMB, resulting in a pronounced absorption peak at 652 nm (Figure S7).[31] The absorbance at 652 nm exhibited a gradual increase over time in the control group, suggesting the production of •OH radicals. Upon the addition of CCzymes to the reaction system, the intensity of the absorption peak progressively diminished in correlation with the concentration of CCzymes, implying a pronounced •OH scavenging effect (Figure 3a,b). Additionally, the electron spin resonance (ESR) spectrum exhibited a reduction in signal intensity when the CCzymes were present, further highlighting their ability to effectively capture and eliminate •OH radicals (Figure 3c).

In biological systems, superoxide dismutase (SOD) plays a pivotal role in the neutralization of ROS by catalyzing the conversion of superoxide anion ($\bullet O_2^-$) into molecular oxygen (O_2) and hydrogen peroxide (H_2O_2). To assess the SOD-like activity of CCzymes, we employed the nitro tetrazolium blue chloride (NBT) method. The scavenging of $\bullet O_2^-$ effectively prevented its reaction with NBT, resulting in the absence of the characteristic blue formazan compound (with a peak at 560 nm) (Figure S8). As depicted in Figure 3d,e, the reaction system without the addition of CCzymes demonstrated a progressive increase in absorbance at 560 nm due to the reduction of NBT by $\bullet O_2^-$. Conversely, the presence of CCzymes resulted in a sharp decrease in absorbance at 560 nm, confirming the dismutation of $\bullet O_2^-$ by CCzymes. Furthermore, the significant SOD-like activity of CCzymes was evident in the ESR spectrum of $\bullet O_2^-$ (Figure 3f). These findings suggest that CCzymes exhibit both remarkable •OH scavenging capability and SOD-like activity (Figure 3g). Specifically, it was highlighted that, at a concentration of 200 μg/mL, CCzymes demonstrated an •OH scavenging rate exceeding 80%, whereas the extract at the same concentration only exhibited a sanitization rate of 19% (Figure 3h). Furthermore, at a concentration of 20 μg/mL, CCzymes displayed an $\bullet O_2^-$ scavenging rate of 98%, surpassing the extract's modest achievement of only 15%. Moreover, the remarkable antioxidant capacity of CCzymes was also demonstrated in the scavenging of the DPPH and ABTS radicals through comparison with CC extract (Figures S9–S11). These results demonstrate that the carbonization of the traditional Chinese herb CC to produce CCzymes can significantly enhance its antioxidant capacity.

The mechanism underlying the antioxidant activity of CCzymes was elucidated by employing Density Functional Theory (DFT) to calculate the reaction pathways of the catalytic cycle. Our recent study demonstrated that carbonyl groups conjugated with the π-system serve as an efficient reaction site in the SOD enzyme activity of CDs.[32] Moreover, extensive research has elucidated that carbonyl groups are prevalent and highly reactive functional groups in CDs, serving as active sites in enzyme-mediated reactions involving •OH.[16, 33] Consequently, we developed a model incorporating carbonyl groups conjugated with the π-system to investigate the catalytic mechanism of CCzymes as a scavenger of •OH and SOD enzymes. The reaction mechanism of CCzymes in terms of the •OH scavenging is illustrated in Figure 3i. Initially, the unbound •OH radical is adsorbed and forms a bond with the carbonyl group (Int* 2). Subsequently, the oxygen atom at the terminal end of the •OH radical reacts with a free proton (H^+) from the surrounding medium, leading to the formation of a water (H_2O) molecule. Finally, the bond between the carbonyl oxygen and the hydrogen atom of the H_2O molecule is cleaved, resulting in the release of the H_2O molecule from the active site. Therefore, the entire process is completed. The energy profile analysis reveals that the adsorption of •OH between Int* 1 and Int* 2 is spontaneous and exothermic, with a calculated energy change of −0.95 eV (Figure 3k). Moreover, the overall reaction is characterized as a reduction in energy, indicating that the presence of CCzymes in the solution facilitates the spontaneous scavenging of •OH without requiring external energy input.

The SOD-like catalytic process of CCzymes is found to be more intricate, as illustrated in Figure 3j. It has been documented that $\bullet O_2^-$, functioning as a Bronsted base,

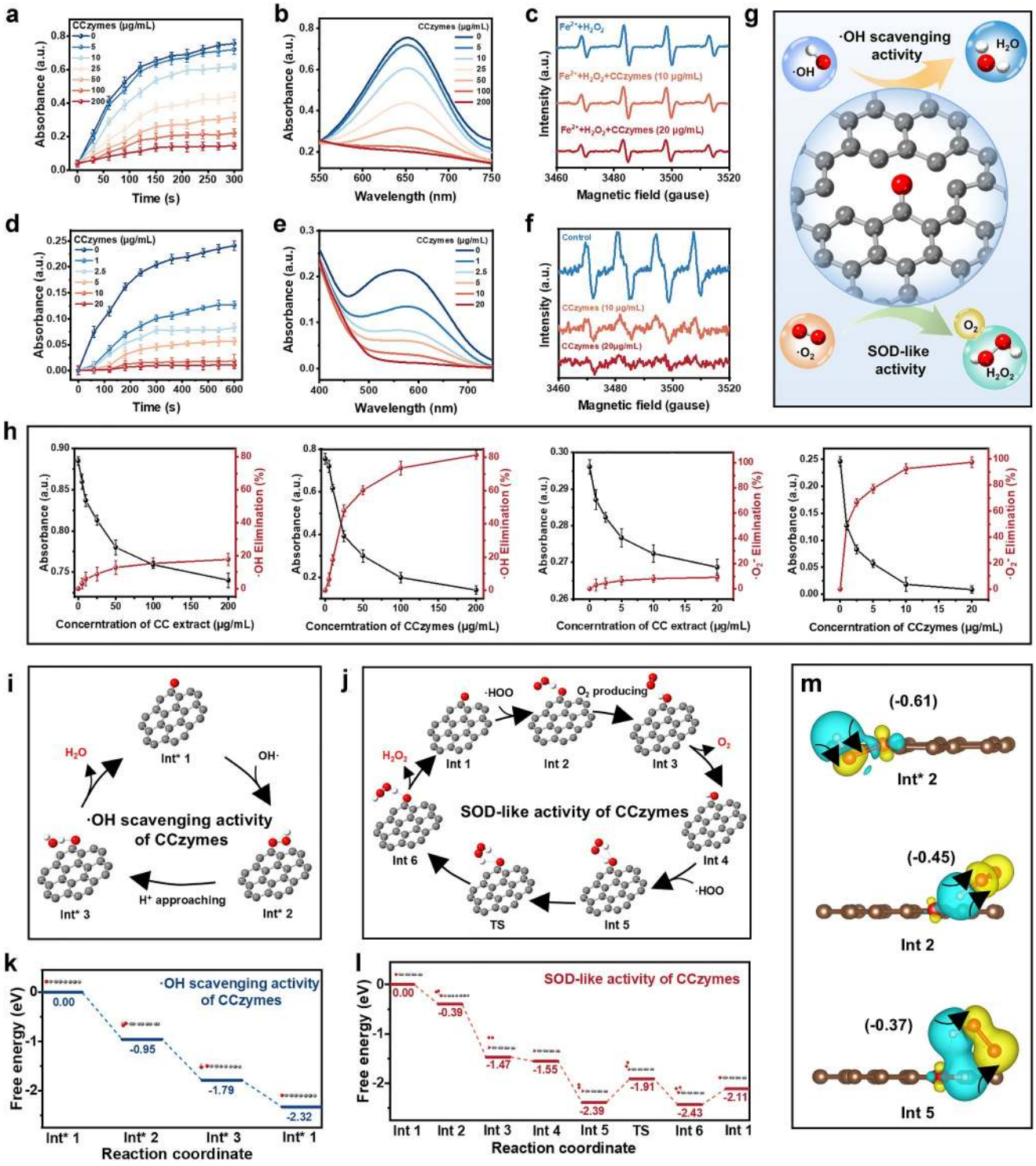

FIGURE 3 Deciphering the catalytic mechanism of CCzymes. (a) Kinetic curves of •OH scavenging, (b) Absorption spectra of oxTMB reacted with •OH, and (c) Electron spin resonance spectrum of •OH at different CCzymes concentrations. (d) Kinetic curves of $•O_2^-$ scavenging, (e) Absorption spectra of NBT reacted with $•O_2^-$ and (f) ESR spectrum of $•O_2^-$ at different CCzymes concentrations. (g) Schematic illustration of the •OH scavenging ability and SOD-like activity of CCzymes. (h) CCzymes and CC extract concentration-dependent elimination efficiencies of •OH and $•O_2^-$. (i) Proposed reaction pathway and (k) Free energy diagram for the •OH scavenging catalytic cycle of CCzymes. (j) Proposed reaction pathway and (l) Free energy diagram for the SOD-like catalytic cycle of CCzymes. (m) The charge density of CCzymes' three states with absorption-free energies is observed during the two catalytic cycles, with yellow and cyan indicating charge accumulation and depletion, respectively. CC, Coptis chinensis.

readily abstracts a proton from the aqueous solution to generate •HOO. Subsequently, the free •HOO is adsorbed and initially bound to a carbonyl group to form an H-O bond. The carbonyl group then oxidizes the •HOO radical, leading to the formation of a hydroxyl group conjugated with the π-system (Int 2→Int 4), while simultaneously producing an O_2 molecule. Additionally, the hydroxyl group within the molecular structure undergoes absorption of a second •HOO molecule, resulting in its conversion back to the original carbonyl structure conjugated with the π-system through hydrogen abstraction. This resulted in the formation of an H_2O_2 molecule (Int 5→Int 1), thereby concluding the entirety of the process. This reaction pathway consists of seven distinct states where the transition states (TS) exhibit intricate structural modifications that enable the CCzymes to carry out cyclic catalysis similar to SOD. The energy profile (Figure 3l) illustrates that the adsorption of •HOO between Int 1 and Int 2 results in a decrease in energy (ΔE: −0.39 eV), suggesting that the adsorption of •HOO by the CCzymes can proceed spontaneously.

The charge-difference density conditions for three states of adsorbed radicals are depicted in the context of the two catalytic cycles (Figure 3m). In Int* 2, the oxygen atom of the absorbed hydroxyl group exhibits charge capture, thereby facilitating its combination with H^+ ions from the surrounding environment. Notably, both Int 2 and Int 5 display substantial charge transfer surrounding the carbonyl group that conjugates with the π-system, serving as a crucial aspect of the catalytic mechanism.[34] This mechanistic study provides compelling evidence that carbonyl oxygen-containing functional groups within the CCzymes act as active sites to facilitate enzyme-catalyzed reactions. According to the aforementioned experimental results, CCzymes exhibit a higher concentration of oxygen-containing functional groups in comparison to CC extract, thereby displaying superior •OH scavenging abilities and SOD-like enzymatic properties. This comprehension facilitates the development of antioxidative nanozymes with improved efficacy through a rational design approach.

2.3 | Antioxidant and anti-inflammatory effects of CCzymes in vitro

UC is a well-known inflammatory disorder characterized by pathological manifestations that are intricately linked to oxidative stress.[35] Overproduction of ROS plays a pivotal role in initiating the inflammatory process.[36] CCzymes happen to demonstrate robust antioxidant enzyme activity. Consequently, our study sought to examine the antioxidant capabilities and cellular protective effects of CCzymes under conditions of oxidative stress. Mitochondria serve as the primary site of ROS generation, thus making them susceptible to initial organelle damage caused by excessive ROS levels. As such, our study first focused on examining the subcellular distribution of CCzymes. We covalently attached the fluorescent dye Sulfo-cy5.5 amine utilizing the carboxyl groups present on the surface of CCzymes via the carbodiimide method. Raw 264.7 cells were co-incubated with the fluorescent CCzymes and the mitochondria of the cells were labeled with Mito-Tracker. The results demonstrated a significant accumulation of CCzymes within mitochondria, as evidenced by a high Pearson's correlation coefficient of 0.96 (Figure 4a–c). This facilitates the mitigation of oxidative stress in cells by CCzymes. The fluorescent probe DHE was employed to assess the levels of $•O_2^-$ in cells, as indicated by its emission of red fluorescence in the presence of $•O_2^-$. Treatment with H_2O_2, an oxidation inducer, notably elevated the levels of $•O_2^-$ in Raw 264.7 cells (Figure 4d and S12a). Subsequently, varying concentrations of CCzymes exhibited differential capacities for scavenging $•O_2^-$. The DCFH-DA probe exhibits green fluorescence in the presence of free radicals, serving as an indicator of cellular oxidative stress. Enhanced green fluorescence in Raw 264.7 cells was observed following its incubation with H_2O_2. Subsequent treatment with varying concentrations of CCzymes resulted in a significant reduction in cellular oxidative stress levels (Figure 4e). The collected cells were subjected to quantitative analysis using flow cytometry, which also revealed that CCzymes exhibited a strong antioxidant effect at the cellular level (Figure 4f). Mitochondria serve as the main source of ROS production and subsequent oxidative damage often arises from mitochondrial impairment.[37] To further investigate the potential of CCzymes in alleviating oxidative stress, we induced oxidative damage in cellular mitochondria using H_2O_2 as an inducer. The state of mitochondria was assessed using the JC-1 probe, wherein red fluorescence indicated the aggregated form of JC-1 and intact mitochondrial membrane potential, while green fluorescence denoted the monomeric form of JC-1 and mitochondrial damage (Figure 4g). The results demonstrate that CCzymes effectively alleviate oxidative damage, maintain the stability of mitochondrial membrane potential, and protect mitochondrial function.

The transformation of macrophage phenotype is mediated by the UC inflammatory immune microenvironment.[38] Remodeling the immune microenvironment at the site of UC inflammation is a key strategy to alleviate UC. CC and its active ingredients have been shown to modulate macrophage polarization. Therefore, we accessed the ability of CCzymes to modulate macrophage

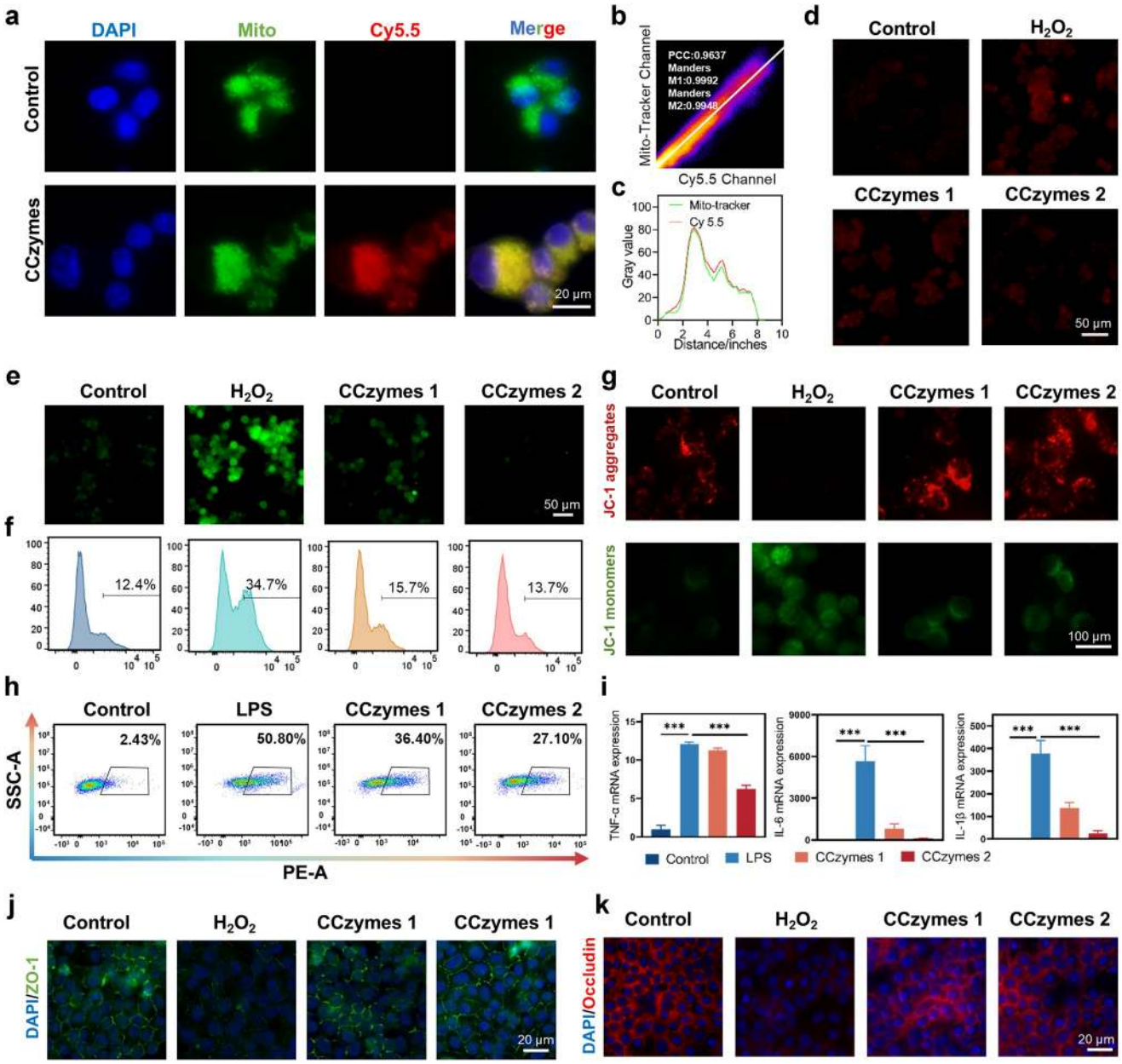

FIGURE 4 Antioxidant and anti-inflammatory properties of CCzymes in vitro. (a) Fluorescence colocalization of CCzymes with mitochondria. (b, c) PCC, Manders' colocalization coefficients, and plot profile corresponding to Figure a. (d) Fluorescence images after incubation of DHE with cells in different groups. (e, f) Fluorescence images and flow analysis results of different groups of cells cultured by DCFH-DA. (g) Fluorescence images of mitochondrial membrane potential repair by CCzymes. (h) Flow analysis results of M1 macrophage polarization in different groups of treatments. (i) mRNA expression level of pro-inflammatory cytokines including TNF-α, IL-6, IL-1β ($n = 3$). (j, k) Immunofluorescence staining images of intestinal tight junction protein expression (ZO-1, Occludin) in different treatment groups. CCzymes 1: inducer +50 μg/mL CCzymes; CCzymes 2: inducer +100 μg/mL CCzymes. Data are expressed as mean ± SD of three independent experiments. Statistical comparisons were made using one-way ANOVA and *t*-test. Statistical significance was indicated as $^{*}p < 0.05$, $^{**}p < 0.01$, $^{***}p < 0.001$, $^{****}p < 0.0001$. CC, Coptis chinensis.

polarization. Specifically, we utilized Lipopolysaccharide (LPS) to co-incubate with Raw264.7 cells to induce their polarization toward M1-type macrophages. The results of flow cytometry analysis showed a significant increase in the expression of M1-type macrophage marker (CD86) upon LPS stimulation. Furthermore, incubation with varying concentrations of CCzymes achieved evident downregulation of CD86 expression, suggesting that the CCzymes can modulate macrophage polarization (Figure 4h and S12b). M1-type macrophages exert pro-inflammatory capacity in the immune microenvironment and can secrete large amounts of pro-inflammatory

cytokines such as TNF-α, IL-1β, and IL-6. Therefore, we further investigated the role of CCzymes in the regulation of pro-inflammatory cytokines expressed by M1-type macrophages. The qPCR analysis revealed a significant up-regulation of pro-inflammatory cytokines in Raw 264.7 cells treated with LPS (Figure 4i). Subsequent treatment with CCzymes led to the restoration of pro-inflammatory cytokine expression. Notably, the higher concentrations of CCzymes were found to be more effective in down-regulating the expression of IL-6 and IL-1β to their baseline levels, a phenomenon seldom observed in our previous work.[39] The above findings demonstrate that CCzymes not only possess antioxidant enzyme activity but also the ability to modulate macrophage polarization and alleviate cellular inflammation. The multifaceted blockade of the cascade response of inflammation confers significant benefits in the treatment of UC. Additionally, it is widely acknowledged that elevated levels of inflammation during the development and progression of UC contribute to the disruption of intestinal barrier function. This impairment can result in the leakage of pathogenic bacteria into the body, further exacerbating inflammation. Therefore, the restoration of intestinal epithelial function is crucial for the effective treatment of UC. Concerning this issue, we constructed a simulated human intestinal epithelial barrier (IEB) in vitro using Caco2 cells. ZO-1 and Occludin are important tight junction proteins expressed by intestinal epithelial cells. We utilized H_2O_2 as an inducer to stimulate oxidative damage in the intestinal epithelium. Immunofluorescence staining was used to detect the expression of ZO-1 and Occludin, revealing a significant down-regulation in their expression levels. However, the expression of tight junction proteins was restored after CCzymes treatment (Figure 4j,k). This result was also supported by quantitative analysis (Figure S12c,d). CCzymes exhibit excellent resistance to oxidation and repair of damage at the cellular level, which provides a foundation for the treatment of UC.

2.4 | RNA sequencing to explore biological mechanisms of CCzymes

To further explore the biological mechanisms underlying the antioxidant and anti-inflammatory properties of CCzymes, we conducted RNA sequencing on macrophages treated with either LPS or LPS + CCzymes. The heatmaps fully illustrated the great effects of LPS and CCzymes on the macrophage transcriptome (Figure 5a). Principal component analysis (PCA) further reflected the differences between LPS and CCzymes treatment (Figure 5b). The volcano plot revealed significant alterations in their gene expression, with 426 genes down-regulated and 364 genes up-regulated in the CCzymes group compared with LPS. Among them, some genes associated with inflammation and oxidative stress were labeled. Inflammation-related genes such as Ccl2, Nos2, Il6, and Kit exhibited significant downregulation. Cat, which possesses catalase activity and is closely linked to redox processes, showed obvious upregulation (Figure 5c). The differential genes were subjected to Gene ontology (GO) enrichment analyses, showing enrichment in biological processes related to inflammation, immune response, and innate immunity (Figure 5d). According to the Kyoto Encyclopedia of Genes and Genomes (KEGG) pathway enrichment analysis, the CCzymes treatment affected several pathways, such as TNF, IL-17, and JAK-STAT signaling pathways (Figure 5e). These findings imply that CCzymes exert anti-inflammatory effects by modulating immune-related pathways and regulating the activity of antioxidant enzymes. In addition, differential genes treated with CCzymes showed enrichment for Inflammatory Bowel Disease (IBD), indicating the potential effectiveness of CCzymes in treating UC. Similarly, to verify the pharmacological activity of CCzymes inherited from CC, we investigated the effect of CC extracts on macrophages using KEGG enrichment analysis. The results indicated that the inflammatory pathways primarily affected by the CC extract were the PI3K-Akt and JAK-STAT signaling pathways (Figure 5f). These two inflammatory pathways were significantly enriched in CCzymes treatment, indicating that CCzymes maintain the pharmacological efficacy of CC and have a stronger impact on inflammatory pathways compared to the CC extract. The differential genes of the enriched pathways were analyzed in greater depth, as demonstrated in Figure 5g and S13. This provides a more comprehensive representation of the significant regulation of macrophage inflammatory signaling pathways by CCzymes. LogFC >1.5 or LogFC < −1.5 is considered statistically significant. The CCzymes treatment group exhibited significant down-regulation of all pro-inflammatory key genes in comparison to the LPS treatment group, as evidenced by statistical analysis. Notably, the most substantial alterations in gene expression within the enriched MAPK and PI3K-Akt signaling pathways were observed in the receptor tyrosine kinase (Kit). The transmembrane protein Kit possesses an extracellular ligand domain that binds to its corresponding ligand, thereby activating protein kinase function and modulating intracellular downstream signaling pathways. Research has demonstrated that Kit plays a crucial role in numerous cellular processes, and the signaling cascades it influences have been implicated in various disease pathologies.[40] We confirmed the impact of CCzymes on Kit expression through qPCR (Figure 5h). LPS stimulation boosted Kit expression,

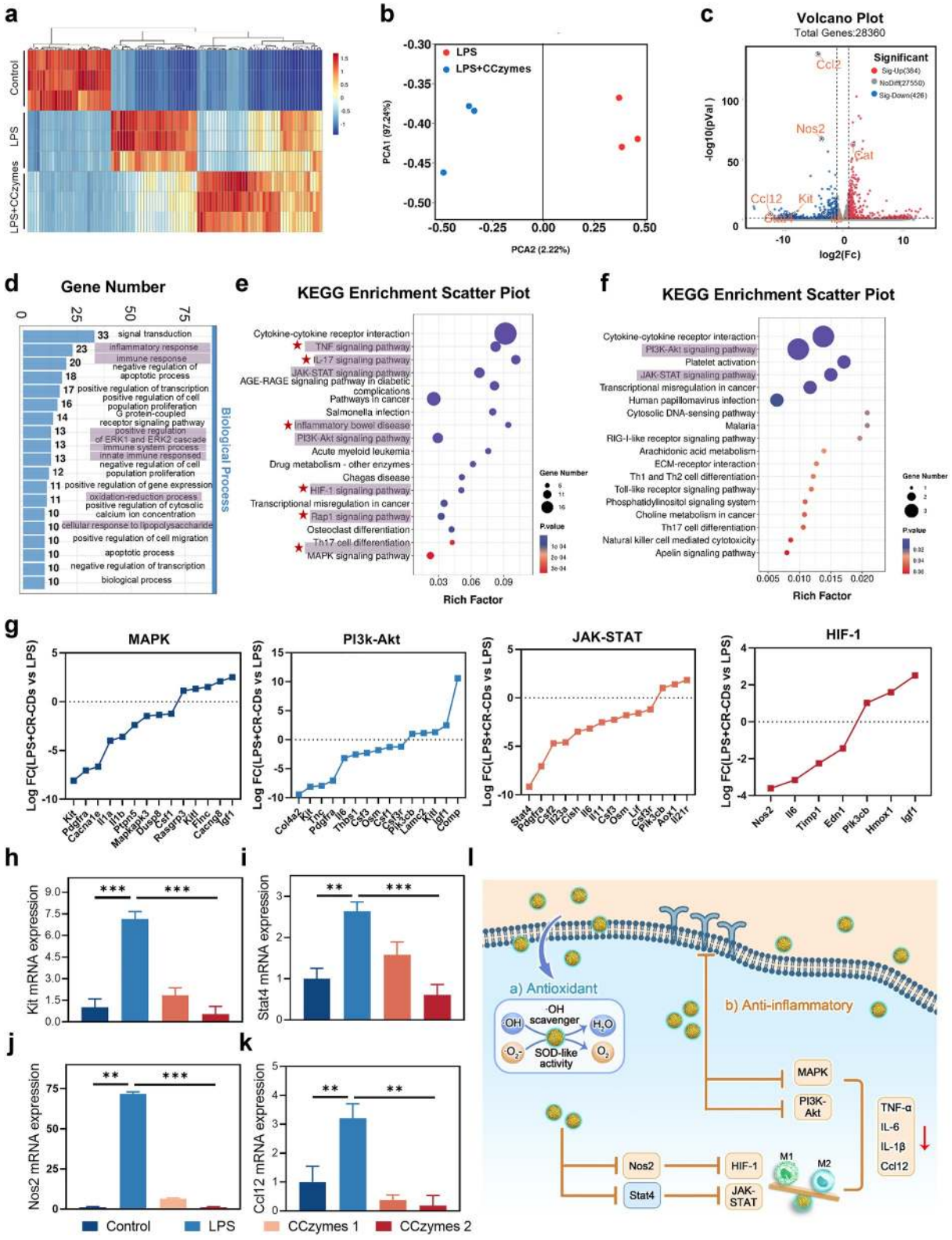

FIGURE 5 Legend on next page.

while both low and high concentrations of CCzymes successfully achieved the down-regulation of Kit. As a key protein, the down-regulation of Kit plays a crucial role in modulating the MAPK and Pl3k-Akt signaling pathways.[41–43] The JAK-STAT and HIF-1 signaling pathways are of interest due to their correlation with macrophage polarization. STAT acts as a transcription factor in the JAK-STAT pathway to regulate gene expression in this process. Additionally, Nos2 within the HIF-1 signaling pathway is identified as a marker for M1-type macrophages.[44] RNA sequencing analysis revealed downregulation of both Stat4 and Nos2 following treatment, which was further confirmed through qPCR analysis (Figure 5i,j). Macrophages release chemokines to attract immune cells for the immune response.[45, 46] CCzymes were found to suppress chemokine expression, as confirmed by qPCR, showing decreased Ccl12 levels in the CCzymes-treated group (Figure 5k). The results indicate that CCzymes have the capacity to inhibit inflammatory signaling pathways such as MAPK and PI3K-Akt by downregulating Kit expression, resulting in decreased pro-inflammatory responses. Furthermore, CCzymes can also suppress JAK-STAT and HIF-1 signaling pathways, thereby influencing the polarization of macrophages toward the M1 phenotype (Figure 5l). In conclusion, CCzymes not only retain the pharmacological activity of CC but also demonstrate enhanced antioxidant and anti-inflammatory properties.

2.5 | In vivo biodistribution of CCzymes

We then studied the metabolism of CCzymes in mice by attaching a fluorescent dye Sulfo-cy5.5 amine. Using a UC mouse model, we injected CCzymes-Cy5.5 intraperitoneally and monitored its distribution over time. The results showed that the fluorescence in the abdomen of mice gradually increased with time, reached a peak value at 30 min, and then began to decrease (Figure 6a). At the same time points, the major organs and colon were imaged ex vivo. The distribution of CCzymes in the organs also demonstrated a trend of increasing and then decreasing. Very little fluorescence was detected in the isolated tissues at 12 h, indicating that CCzymes were successfully metabolized. The fluorescence of isolated tissues was analyzed statistically. The liver and kidney, serving as the principal filtration organs, exhibited a predominant distribution of CCzymes in both healthy and UC group mice, as depicted in Figure 6b,c. CCzymes injected intraperitoneally were absorbed by the superior mesenteric vein and aggregated in the colon. The assessment of pharmacokinetics in vivo is essential for drug screening. Therefore, the CCzymes content in serum was measured from the collected mouse blood. Figure 6d shows the pharmacokinetic profile of CCzymes, with a half-life of ~53 min calculated from the time when the drug concentration reached the maximum value. This indicates that CCzymes can be metabolized out of the blood quickly. Moreover, the drug distribution in the colon site was also counted. Figure 6e and f displays the drug distribution in the colon of healthy and UC mice, respectively. The half-life of CCzymes in the colon was ~43 min in healthy mice and 71 min in UC mice. CCzymes were retained for a shorter period in healthy mice compared to UC mice. The colonic fluorescence at 12 h was further confirmed (Figure 6g). These results may be attributed to a reduction in tight junction proteins at the site of colonic inflammation, an augmented inflammatory response, and an elevation in intestinal permeability.

2.6 | Therapeutic efficacy of CCzymes against acute UC

Inspired by the excellent antioxidant and anti-inflammatory effects of CCzymes in vitro, the therapeutic effect of CCzymes against acute UC in vivo was investigated. Multiple groups were established for the study, including healthy mice (G1), saline-treated acute UC mice (G2), acute UC mice treated with 10 mg/kg CC extract (G3), acute UC mice treated with low-dose 5 mg/kg

FIGURE 5 RNA sequencing to explore the biological mechanisms of CCzymes. (a) Heat map of genes in different treatments. (b) Principal component analysis of the LPS + CCzymes group and the LPS group. (c) Volcano plots of all genes in the LPS + CCzymes group and the LPS group. The red dots represented the upregulated differently expressed genes, the blue dots were downregulated differently expressed genes, and the gray dots were non-differentially expressed genes. (d, e) GO and KEGG enrichment of differential genes in LPS + CCzymes and LPS groups. (f) KEGG enrichment of differential genes in LPS + CC extract and LPS groups. (g) Expression levels of differentially expressed genes in different signaling pathways. (h–k) Expression of cytokines Kit, Stat4, Nos2, and Ccl12 in different treatment groups ($n = 3$). (l) Schematic illustration of the anti-inflammatory and antioxidant mechanism of CCzymes. Data are expressed as mean ± SD of three independent experiments. Statistical comparisons were made using one-way ANOVA and *t*-test. Statistical significance was indicated as $^{*}p < 0.05$, $^{**}p < 0.01$, $^{***}p < 0.001$, $^{****}p < 0.0001$. CC, Coptis chinensis; GO, Gene ontology; KEGG, Kyoto Encyclopedia of Genes and Genomes.

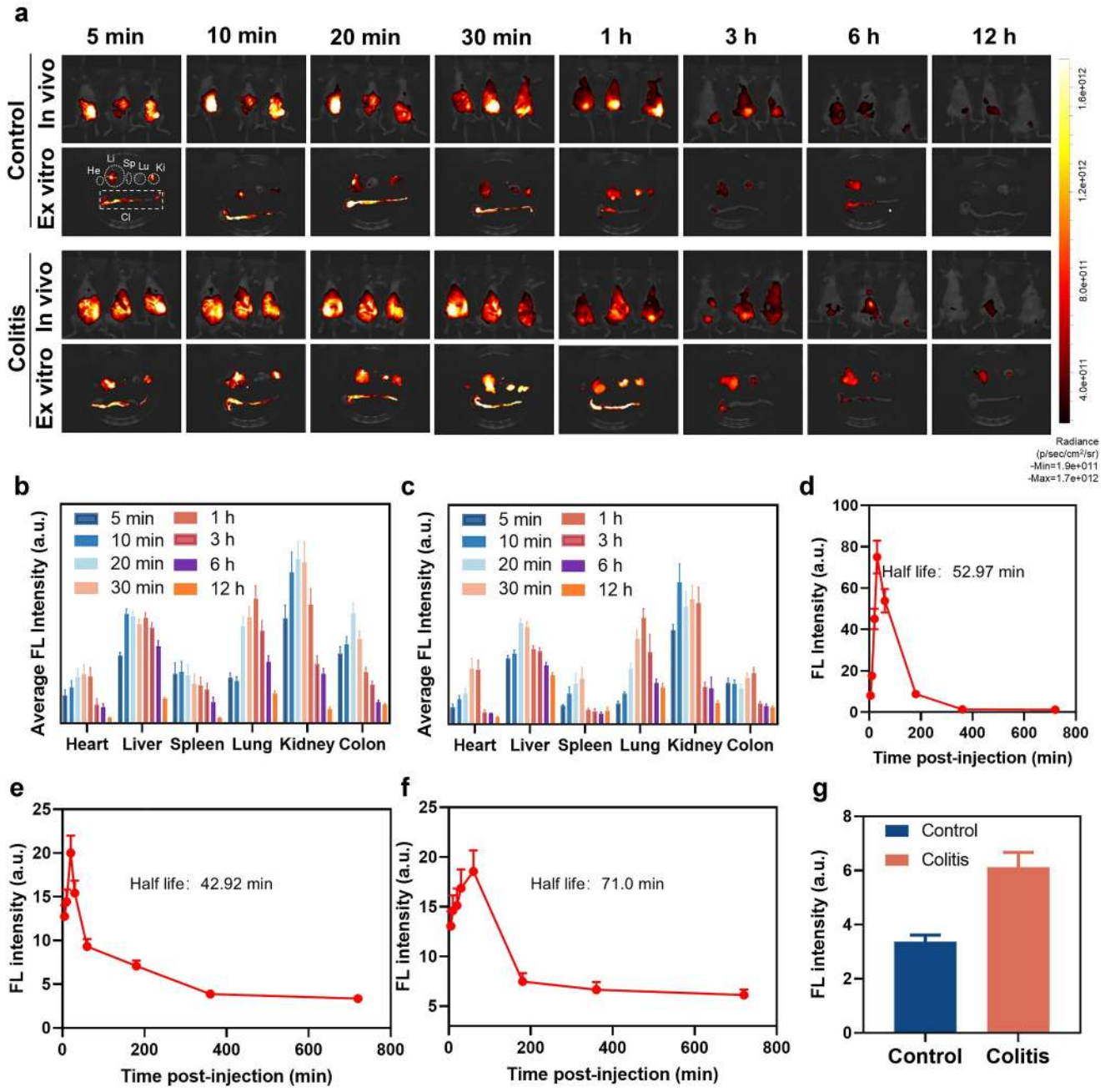

FIGURE 6 Biodistribution of CCzymes. (a) In vivo and ex vivo imaging of CCzymes at the different time points in healthy and UC mice. Ex vivo imaging includes the heart, liver, spleen, lung, kidney, and colon. (b, c) Fluorescence statistics of CCzymes in different organs of mice in healthy and colitis groups. (d) Pharmacokinetic curve of CCzymes in the blood. (e) Distribution of CCzymes in the colon of mice in the healthy group over time. (f) Distribution of CCzymes in the colon of mice in the UC group over time. (g) Comparison of colonic fluorescence between healthy and UC group mice at 12 h ($n = 3$). CC, Coptis chinensis; UC, ulcerative colitis.

CCzymes (G4), and acute UC mice treated with high-dose 10 mg/kg CCzymes (G5). The acute UC model was constructed by giving mice 2.5% Dextran Sulfate Sodium Salt (DSS) for 7 consecutive days. The experimental procedure is illustrated in Figure 7a, depicting the progression of the experiment. The body weight and Disease Activity Index (DAI) scores of the mice were regularly recorded throughout the process to assess the development of acute UC and the efficacy of the different treatments. It was evident that the mice with acute UC exhibited a significant decrease in body weight compared to the control group (Figure 7b). Specifically, the acute UC mice without any treatment demonstrated the most substantial decrease in body weight, decreasing from 19.54 ± 0.82 g to 16.34 ± 0.68 g. The body weight of mice treated with CC extract decreased from 19.26 ± 0.42 g to 16.7 ± 0.46 g, with

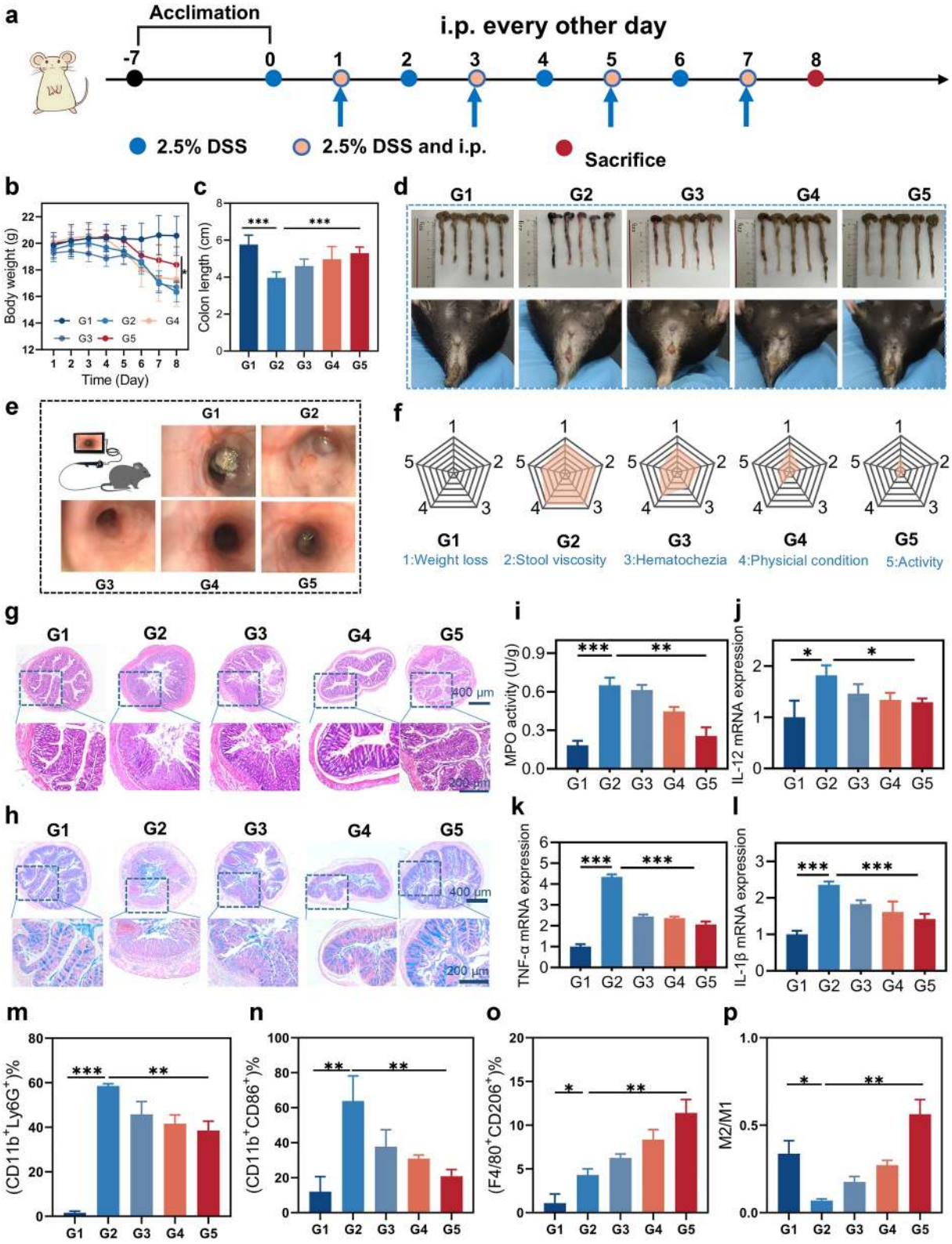

FIGURE 7 Legend on next page.

limited therapeutic efficacy observed. Interestingly, the therapeutic impact of CCzymes became increasingly evident with higher concentrations. The body weight of mice in the G5 group was recorded as 18.38 ± 1.2 g on Day 8. On the same day, the colons of mice from various treatment groups were extracted and measured. It was observed that the colon length of mice in the acute UC group was significantly reduced to 3.96 ± 0.28 cm in comparison to the healthy group, which had a colon length of 5.77 ± 0.47 cm. The colon length in G5 group mice was restored to 5.3 ± 0.3 cm (Figure 7c). The ex vivo images of the colons of mice in various treatment groups on Day 8, as well as the presence of blood in the stools of mice, were also displayed (Figure 7d). The visual evidence provided a valuable contribution to the comprehension of the successful modeling of acute UC in mice and underscored the significant therapeutic impact of CCzymes. In clinical practice, ulcerated colons of UC patients are typically observed during endoscopy. Hence, on Day 8 of the experiment, a microscopic examination of the colons of mice was conducted using a small animal endoscope, which illustrated the presence of discernible ulcers in the colons of mice induced with DSS. A distinct whitish hue of the colonic inner surface was observed in the mice from the acute UC group compared to those in the healthy group, indicating the presence of inflammation. Additionally, the clarity of blood vessels on the colonic inner surface of mice treated with CC extract was diminished. Conversely, mice treated with varying concentrations of CCzymes exhibited a significant improvement in colonoscopic condition (Figure 7e). In the course of the experiment, we constructed a 5-sided scoring system based on five aspects of weight loss, stool viscosity, hematochezia, physical condition, and activity to score mice for DAI. As shown in Figure 7f, the DAI scores of mice in the high-concentration CCzymes treatment group exhibited remarkable proximity to those observed in the healthy group. Hematoxylin and eosin (H&E) staining of colonic tissues of mice in different treatment groups was used to assess the degree of damage to colonic tissues as shown in Figure 7g. Colonic crypts were significantly lost and intestinal epithelial tissues were significantly damaged in the acute UC group of mice. Recovery of the colonic crypts was not fully achieved in the CC extract-treated group, and a large infiltration of immune cells was still observed in the H&E results. On the contrary, after CCzymes treatment, the crypts and intestinal epithelium of the colon tissue were significantly restored. Alcian blue-Periodic acid Schiff (AB-PAS) staining was used to assess the distribution of tissue glycogen and polysaccharides, which indicated the expression of occludin proteins and mucins in colonic tissues. Downregulation of occludin protein and mucin represents damage to the intestinal barrier. Upon comparison, it was evident that significant intestinal barrier damage occurred in the acute UC group, and CCzymes treatment restored the integrity of the intestinal barrier (Figure 7h). Myeloperoxidase (MPO) is a class of oxidoreductase enzymes secreted by neutrophils during the onset of inflammation. MPO stimulates the production of ROS. At sites of inflammation, MPO was used to indicate the level of oxidative stress. We collected mucosal tissue from the colon for the measurement of MPO. The results showed that MPO levels in the colon decreased after CCzymes treatment, providing compelling evidence for the antioxidant enzyme activity of CCzymes in alleviating the level of oxidative stress in the acute UC (Figure 7i). The observed variations in pro-inflammatory cytokines IL-12, TNF-α, and IL-1β confirmed the presence of inflammation in the colon of mice in the acute UC group. Remarkably, administration of CCzymes significantly attenuated the expression of these pro-inflammatory cytokines (Figure 7j–l). The results demonstrated an evident inhibition of inflammation by CCzymes. To further evaluate the efficacy of CCzymes in treating acute UC, we performed a flow cytometry analysis of the infiltration of immune cells in the colon tissue. Neutrophils, as innate immune effector cells, accumulate in substantial quantities and infiltrate mucosal epithelial cells during colonic inflammation. Neutrophil markers $CD11b^+$ and $Ly6G^+$ were labeled for flow sorting. The results showed that acute UC mice had massive aggregation of neutrophils, which were significantly downregulated in the treatment group (Figure 7m

FIGURE 7 Therapeutic efficacy of CCzymes on acute UC. (a) The schematic diagram shows the full procedure of the experiment ($n = 5$). (b) Daily body weight over 8 days (c) Measurements of colon lengths after different treatments. (d) Photographs of colon and blood in stool in different treatment groups. (e) Representative photos of the intestinal endoscope of mice treated with the indicated materials on Day 8. (f) Disease Activity Index scores in the different treatment groups during treatment. (g, h) H&E and Alcian blue-Periodic acid Schiff stained colon pathology sections of mice treated with the indicated materials on Day 8. (i) Activity of MPO in different treatment groups. (j–l) Levels of mRNA expression of IL-12, TNF-α, and IL-1β in colon tissues. (m–o) Flow analysis statistics of neutrophils and M1/M2 macrophages in colon tissues of different treatment groups. (p) Statistics on the ratio of M1/M2 macrophages in different treatment groups. G1: Control; G2: DSS; G3: DSS+10 mg/kg CC extract; G4: DSS+5 mg/kg CCzymes; G5: DSS+10 mg/kg CCzymes. Data are expressed as mean ± SD of three independent experiments. Statistical comparisons were made using one-way ANOVA and *t*-test. Statistical significance was indicated as $^*p < 0.05$, $^{**}p < 0.01$, $^{***}p < 0.001$, $^{****}p < 0.0001$. CC, Coptis chinensis; UC, ulcerative colitis.

and S14a). Similarly, the colonic area exhibited a significant increase in both the types and quantities of macrophages during inflammation. The aforementioned in vitro experiments have demonstrated that CCzymes can regulate macrophage phenotypes through the JAK-STAT and HIF signaling pathways. Therefore, we further validated these findings by labeling markers $CD11b^+$ and $CD86^+$ in M1-type macrophages and $F4/80^+$ and $CD206^+$ in M2-type macrophages for sorting in flow cytometry. The results indicated that the CCzymes with a high concentration exhibited the most potent inhibition of M1-type macrophages (Figure 7n and S14b). Additionally, there was a gradual increase in the number of M2-type macrophages as the treatment concentrations escalated (Figure 7o and S14c). Subsequently, we performed a detailed analysis and quantification of the M2 to M1-type macrophage ratio (Figure 7p). It was observed that the group treated by the CCzymes with a high concentration exhibited a higher proportion of M2-type macrophages compared to the healthy group, which had a positive effect on promoting the reduction of inflammation. In conclusion, CCzymes exhibited anti-inflammatory effects by regulating oxidative stress and modulating macrophage polarization, thereby inhibiting the infiltration of inflammatory cells. These findings suggest that CCzymes retain the therapeutic properties of CC and demonstrate improved efficacy in treating UC compared with CC extract.

2.7 | Therapeutic efficacy of CCzymes against chronic UC

UC is typically identified by persistent intestinal inflammation, prompting us to develop a chronic UC model to assess the therapeutic efficacy of CCzymes. Mice were administered a 2% DSS solution in their drinking water, with a regimen consisting of 5 days of DSS water followed by 3 days of pure water every 8 days, repeated for a total of four cycles over 30 days. This model was designed to replicate the chronic inflammatory nature of UC observed in clinical settings, characterized by recurrent episodes of inflammation. CC extract and CCzymes were administered by intraperitoneal injection to chronic UC mice every 3 days. In this experiment, we also set up the same five groups as the acute UC mice, including healthy mice (G1), saline-treated chronic UC mice (G2), 10 mg/kg CC extract-treated chronic UC mice (G3), low-dose 5 mg/kg CCzymes-treated chronic UC mice (G4), and high-dose 10 mg/kg CCzymes-treated chronic UC mice (G5). The schematic diagram in Figure 8a shows the flow of this experiment.

Figure 8b illustrates the body weight changes of the mice in each group during the treatment process. The results revealed that the mice in the chronic UC group showed the most significant weight loss during the experiment. The administration of high concentrations of CCzymes most significantly inhibited the rapid weight loss of mice. On Day 30, the body weight of mice in the high-concentration CCzymes treatment group was significantly higher than that of mice with UC. Figure 8c and d shows the length statistics and photographs of isolated colon tissues of mice, respectively. The recovery of colon length was most pronounced after treatment with a high concentration of CCzymes. Similarly, the mice were subjected to in vivo endoscopy before sampling on day 30. The mice in the chronic UC group exhibited the most severe colonoscopy findings, characterized by multiple bleeding spots. Among the three treatment groups, the mice receiving high-concentration treatment demonstrated superior colon recovery, as evidenced by prominent blood vessels observed under microscopic examination (Figure 8e). The H&E stained pathology images depicted in Figure 8f indicated the pronounced therapeutic effect of the high-concentration CCzymes, by exhibiting clear crypts and intact intestinal epithelial cells. AB-PAS staining assay was used to assess the integrity of the colonic epithelial mucosa (Figure 8g). It was shown that the down-regulation of mucin occurred in the chronic UC model. However, significant recovery of occludin and mucin expression was observed following CCzymes treatment. Additionally, the antioxidant effect of CCzymes led to a decrease in the MPO content at the site of colonic inflammation (Figure 8h). Malondialdehyde (MDA) is one of the main products of lipid peroxidation, and its concentration can serve as an indirect indicator of redox status. The experimental results showed that MDA levels in the CCzymes treatment group decreased and even returned to normal (Figure 8i). This is attributed to the excellent antioxidant enzyme activity of CCzymes. The pro-inflammatory cytokines IL-12, TNF-α, and IL-1β in the colon tissue were used to indicate the inflammatory state of the colon. In chronic UC, DSS significantly upregulated the level of inflammation. However, pro-inflammatory cytokines in the CCzymes-treated group were similar to those in the healthy group of mice, suggesting that CCzymes also demonstrated an inflammation-reducing effect in chronic UC (Figure 8j–l). The protection of the intestinal mucosal barrier favors the restoration of colonic inflammation. Immunofluorescence staining for intestinal tight junction proteins ZO-1, Claudin 1, and Occludin was used to indicate the function of the intestinal barrier. Similarly, treatment with CCzymes restored the expression of intestinal tight junction proteins ZO-1, Claudin 1, and Occludin (Figure 8m). This result is further supported by fluorescence quantification (Figure 8n and S15). It is worth noting that the therapeutic efficacy of the CC extract was consistently unsatisfactory in the treatment of chronic UC. All

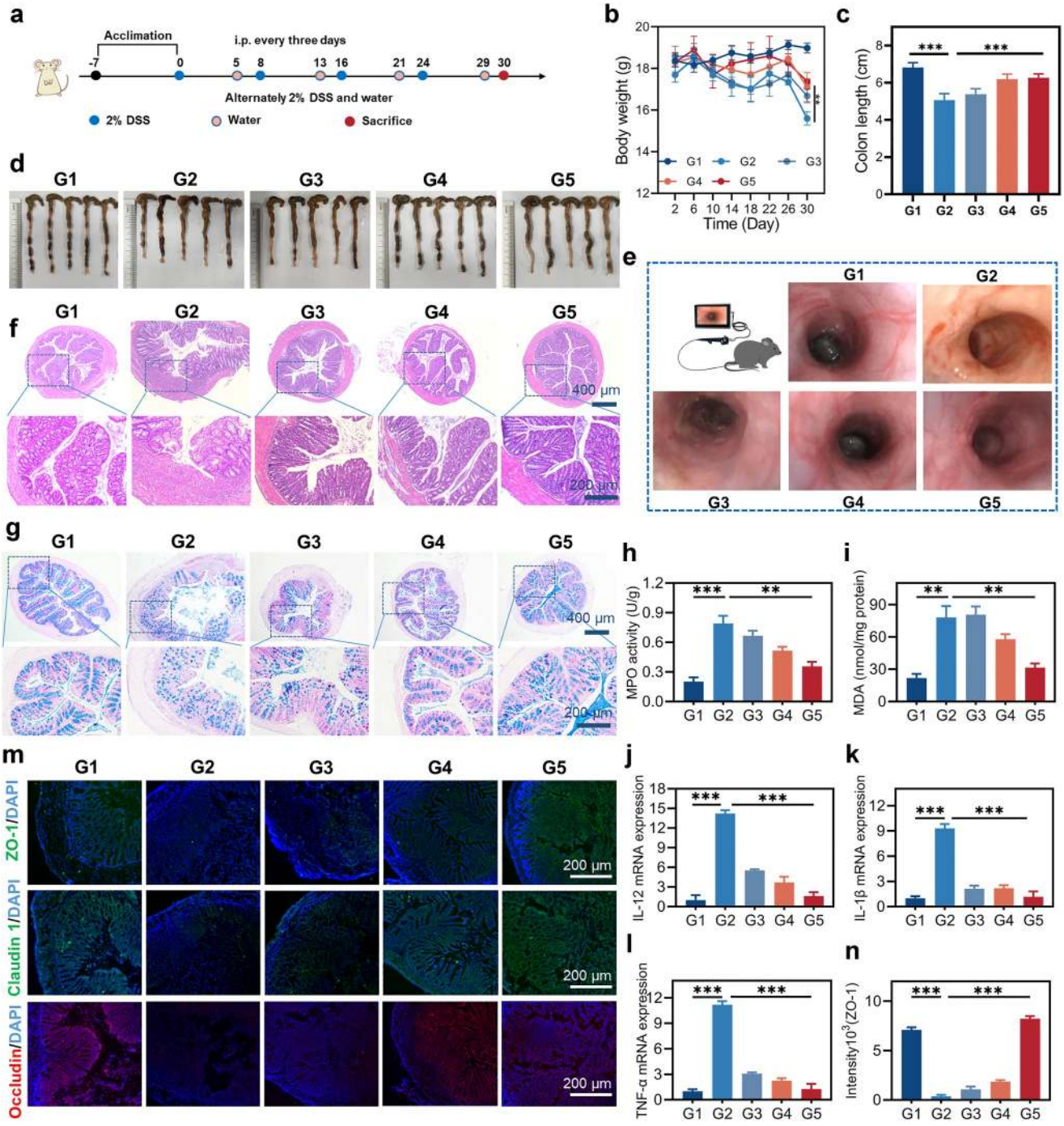

FIGURE 8 Therapeutic efficacy of CCzymes in chronic UC. (a) A schematic diagram shows the full procedure of the experiment ($n = 5$). (b) Daily body weight over 30 days (c) Measurements of colon lengths after different treatments. (d) Photographs of the colon in different treatment groups. (e) Representative photos of the intestinal endoscope of mice treated with the indicated materials on Day 30. (f, g) H&E and Alcian blue-Periodic acid Schiff stained colon pathology sections of mice treated with the indicated materials on Day 30. (h) The activity of MPO in different treatment groups. (i) MDA content in the colon of different treatment groups. (j–l) Levels of mRNA expression of IL-12, IL-1β, and TNF-α in colon tissues. (m) Immunofluorescence staining of tight junction proteins (ZO-1, Claudin 1, and Occludin) in the colon of different treatment groups. (n) Statistics of ZO-1 immunofluorescence staining in different treatment groups. G1: Control; G2: DSS; G3: DSS+10 mg/kg CC extract; G4: DSS+5 mg/kg CCzymes; G5: DSS+10 mg/kg CCzymes. Data are expressed as mean ± SD of three independent experiments. Statistical comparisons were made using one-way ANOVA and *t*-test. Statistical significance was indicated as $^{*}p < 0.05$, $^{**}p < 0.01$, $^{***}p < 0.001$, $^{****}p < 0.0001$. CC, Coptis chinensis; UC, ulcerative colitis.

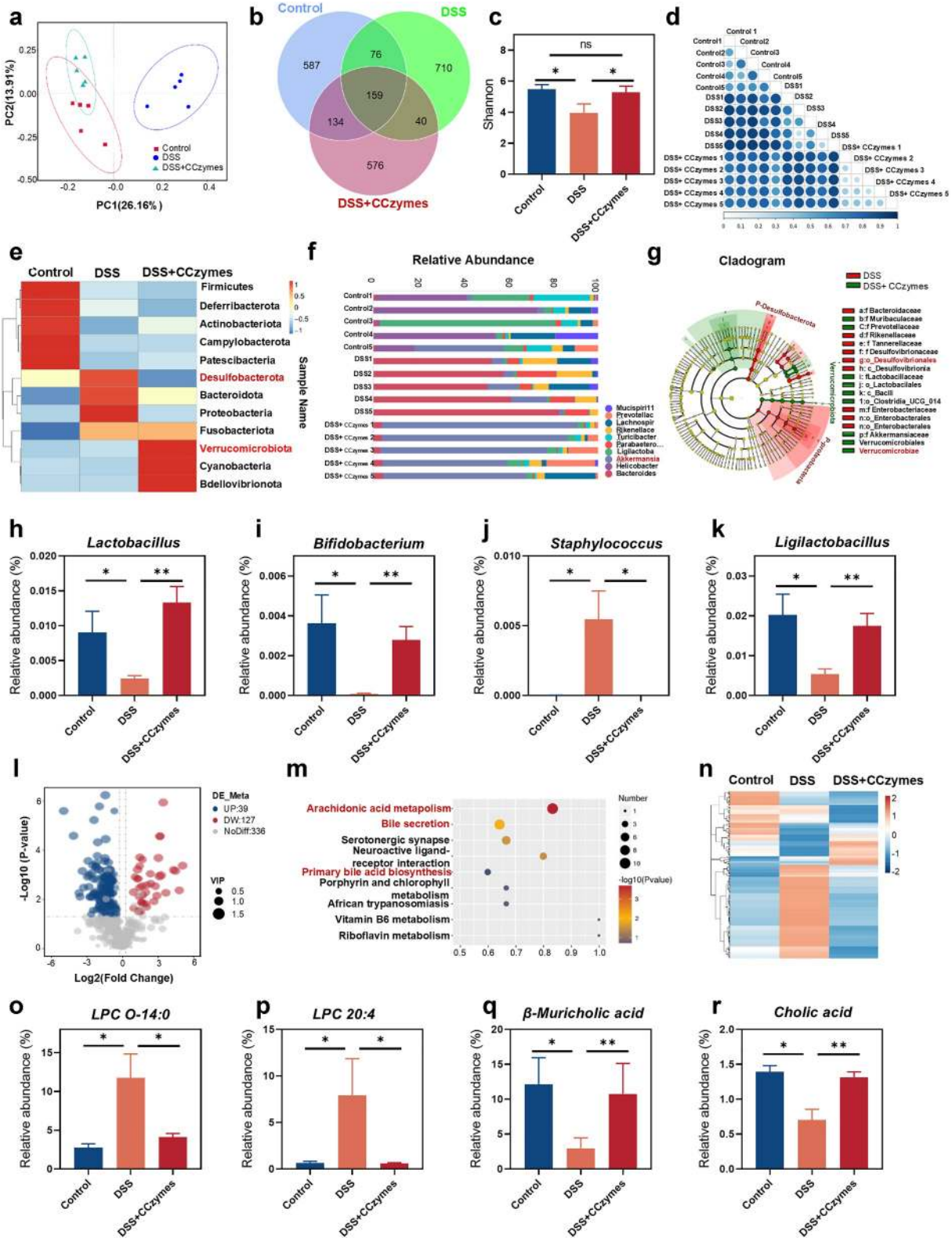

FIGURE 9 Legend on next page.

these findings suggest that the administration of CCzymes effectively restores the intestinal barrier and alleviates chronic UC.

2.8 | Regulation of gut microbiota and metabolites in chronic UC by CCzymes

Studies have shown that the onset and progression of intestinal diseases are closely linked to the gut microbiota.[47] The gut microbiota and its metabolites can mediate the host's inflammatory response and immune system. Berberine, the active ingredient in Coptidis Chinensis, has been shown to alleviate UC by modulating the diversity and species structure of the gut microbiota.[48] Therefore, we analyzed the gut microbiota composition of mice with chronic UC to investigate the regulation of gut microbiota and its metabolites by CCzymes. Using 16S rRNA technology, PCA revealed that the microbiota structure of the CCzymes-treated group had a high similarity to that of the healthy group of mice (Figure 9a). The results from the Venn diagrams demonstrated that there were more intersections in the gut microbiota between the CCzymes-treated group and the healthy group of mice compared to those in the chronic UC group (Figure 9b). The Alpha Diversity Index was used to analyze whether there was a significant difference in species richness among these groups. As depicted, there was no notable difference in the alpha diversity index between the healthy group and the CCzymes-treated group, indicating comparable species richness between the two groups (Figure 9c). However, the alpha diversity index of the chronic UC group was significantly different from both of the other two groups. β-diversity shows the composition of the microbial community in the different samples (Figure 9d). The darker colors represent greater variability while the lighter colors represent less variability. The analysis revealed reduced variability within the three treatment groups, with less variability observed between the CCzymes-treated group and the healthy group compared to that between the chronic UC group and the other two groups. In addition, the heat map of species abundance at the gate level showed a significant increase in the abundance of the beneficial bacterium Verrucomicrobiota (metabolism-friendly probiotic) in the CCzymes-treated group (Figure 9e). Conversely, Desulfobacterota, a harmful bacterium known to trigger inflammatory responses in the gut, was significantly up-regulated in the chronic UC group, whereas a significant down-regulation of Desulfobacterota was observed in the CCzymes-treated group. Next, we performed species abundance analysis at the genus level (Figure 9f). It was seen that the beneficial bacterium Akkermansia was up-regulated in the CCzymes-treated group. Akkermansia belongs to the genus Verrucomicrobiota. In addition, species branching evolution and Linear Discriminant Analysis (LDA) further supported the significant increase in Verrucomicrobiae observed specifically in the CCzymes-treated group (Figure 9g). Figure 9h–k reveals the comparison of the abundance of harmful and beneficial bacteria in the different groups. The beneficial bacteria *Lactobacillus*, Bifidobacterium, and Ligilactobacillus, which are capable of secreting short-chain fatty acids, were all successfully restored following the treatment with CCzymes, whereas the pathogenic bacterium *Staphylococcus* exhibited a significant down-regulation. On the contrary, the pathogenic bacteria *Escherichia-Shigella*, *[Ruminococcus] torques group*, and *Mucispirillum* were up-regulated in the chronic UC group and down-regulated after CCzymes treatment (Figure S16a–c). These results suggest that CCzymes demonstrate specificity in the regulation of gut microbiota. CCzymes can inhibit the growth of pathogenic bacteria while promoting the growth of probiotics. The metabolic pathways and biological functions of a microbiome can be predicted based on the genomic information of a given biome. Therefore, we performed functional prediction based on the results of 16S rRNA. The results of PCA showed that the healthy group and the CCzymes-treated group had a higher abundance of shared functionality, whereas the chronic UC group displayed a decreased

FIGURE 9 Regulation of gut microbiota and gut metabolites by CCzymes. (a) Principal component analysis of different treatment groups. (b) Veen plots demonstrate the intersection of bacterial colony structures in different treatment groups. (c) The Alpha Diversity Index shows the diversity of the microbial community. (d) Diversity index analysis based on the unweighted unifrac distance matrix heatmap. (e) Heat maps of the structure of the Phylum-level microbiota in different treatment groups. (f) Histogram of colony structure at the genus level for different treatment groups. (g) Evolutionary branching diagram with circles radiating from the inside to the outside representing the taxonomic rank from phylum to genus (or species). (h–k) Comparison of abundance of key bacteria in different treatment groups ($n = 3$). (l) Metabolomics volcano plots of DSS and DSS + CCzymes groups. (m) Kyoto Encyclopedia of Genes and Genomes analysis of differential metabolites in different treatment groups. (n) Heat map of differential metabolites in different treatment groups. (o–r) Abundance statistics of major differential metabolites in different treatment groups ($n = 3$). Data are expressed as mean ± SD of three independent experiments. Statistical comparisons were made using one-way ANOVA and *t*-test. Statistical significance was indicated as $^{*}p < 0.05$, $^{**}p < 0.01$, $^{***}p < 0.001$, $^{****}p < 0.0001$.

presence of such functionality, potentially attributed to an elevated prevalence of pathogenic bacteria within this particular group (Figure S16d). In recent years, many studies have reported that microbial metabolites in the gastrointestinal tract, such as bile acids, short-chain fatty acids, and indoles, exert a regulatory effect on inflammation and the immune system within the gut.[49] Therefore, we investigated the variation of metabolites among different groups of mice using untargeted metabolomics to confirm the therapeutic efficacy of CCzymes. As shown in the volcano plot in Figure 9l, the metabolites in the CCzymes-treated group showed significant changes compared to the chronic UC group, with 39 up-regulated and 127 down-regulated. Enrichment analysis of the differential metabolites showed that the differential metabolites were associated with Arachidonic acid metabolism, Bile secretion, and Primary bile acid biosynthesis (Figure 9m). The heatmap in Figure 9n suggested that the most pronounced metabolite changes were observed in the chronic UC group, potentially due to the increase in the number of harmful bacterial species. However, the differential metabolites in the CCzymes-treated group were similar to those in the healthy group, suggesting that the modulatory effect of CCzymes was effective. In particular, lysophosphatidylcholine (LPC) was down-regulated in the CCzymes-treated group compared to the chronic UC group, whereas several indole and cholic acid derivatives were up-regulated (Figure 9o–r and S17). LPC has been reported to be prone to stimulate the onset and development of intestinal inflammation as a harmful metabolite.[50] Indole derivatives, which are catabolic metabolites of the microbial tryptophan metabolism, exhibit protective effects against UC and help maintain the biological integrity of the human gut. Additionally, cholic acid and its derivatives are emerging as promising candidates for UC treatment. In summary, CCzymes can alleviate UC by specifically regulating the composition and structure of the gut microbiota, as well as regulating gut metabolites.

2.9 | Biosafety evaluation of CCzymes

Nanotoxicology has been a major concern in the application of nanomedicine to clinical settings. Consequently, we performed comprehensive biosafety assessments at both cellular and animal levels. The MMT assay was used to test the biocompatibility of CCzymes on cells. Raw264.7 and Caco2 cell lines were exposed to varying concentrations of CCzymes for 12 and 24 h, respectively. Notably, even when the concentration of CCzymes reached 100 μg/mL and the incubation time was extended to 24 h, both cell lines exhibited a remarkable survival rate of 100% (Figure S18a,b). This finding strongly supports the potential utilization of CCzymes in nanomedicine across cellular and animal models. In addition, the hemolysis of CCzymes in the blood was also verified. As shown in Figure S18c, there was no significant hemolysis of blood cells as the concentration of CCzymes increased. Flow analysis of calcein-AM/PI co-staining further verified the good biocompatibility of CCzymes (Figure S18d). Next, the biosafety of CCzymes in mice was systematically investigated. c57BL/6 mice were injected intraperitoneally with 10 mg/kg of CCzymes every other day until the mice were executed on the eighth day. Blood and major organs of the mice were collected for subsequent analysis. We performed H&E staining pathology analysis of the heart, liver, spleen, lungs, and kidneys of the mice. As shown, there were no significant tissue changes or cellular damage in the major organs of mice in the CCzymes administration group compared to mice in the control group (Figure S19a, b). The collected blood was also analyzed for blood biochemistry and hematology. Compared to the control group of mice, there were no significant differences in serum total protein (TP), serum albumin (ALB), globulin (GLO), albumin transaminase (AST), urea nitrogen (UREA), and glucose (GLU) in the blood biochemistry indices (Figure S20a). The obtained indexes demonstrated that CCzymes did not induce significant hepatic and renal impairments in mice, which is advantageous for their potential clinical application. Additionally, as shown in Figure S20b, there was also no significant change in the blood routine indexes of leukocytes, erythrocytes, lymphocytes, hemoglobin, neutrophils, and platelets. These findings collectively validate the favorable biosafety profile of CCzymes at both cellular and animal levels.

3 | DISCUSSION

With the development of nanotechnology, nanozymes with different enzyme activities for different diseases have been developed. Li et al.[51] synthesized metal-based nanozyme Pd/CoPcS-TiCTx using Pd, Co, and TiCTx. By purposeful design, Pd/CoPcS-TiCTx showed strong superoxide dismutase (SOD) and catalase mimicry (CAT), which plays a great role in the treatment of osteoarthritis (OA). Yang et al. developed a Cu-based superoxide dismutase (SOD)-mimicking enzyme with coordinately unsaturated Cu-N_4 single-atom sites to efficiently scavenge excessive ROS (RONS), thereby treating sepsis by interrupting free radical chain reactions and alleviating inflammation.[52] Ye et al. developed a Pt-NC single-atom nanozyme.[53] Due to the ultra-high specific surface area and synergistic effect, the single-atom nanozyme has a higher ROS scavenging ability compared to nanoclusters. Pt-NC has a very good protective effect against reperfusion injury in myocardial ischemia. In tumor therapy, nanozymes with multiple enzymatic activities have been

equally developed. Fan et al.[54] used nitrogen-doped porous carbon nanospheres to develop artificial enzymes with OXD, POD, CAT, and SOD. Directed by ferritin, the nanozymes produced ROS specifically at the tumor site leading to significant tumor therapeutic effects. Wu et al.[55] designed and developed a novel nano-enzyme with NADPH-mimicking oxidase. The nanozymes were able to prevent the regeneration of GSH and inactivate GPX4 through catalytic NADPH depletion, ultimately promoting the iron death of tumor cells. In 2023, Gao et al.[56] first introduced the concept of CDs nanozymes. It has been shown that hydroxyl, amino, carboxyl, and carbonyl groups on the surface of CDs play a great role in mimicking enzyme activity. The mechanism of action of the CD nanozyme continues to be revealed. Yang et al.[57] synthesized nanodots using natural polyphenols with ultrahigh antioxidant capacity, which play a huge role in the treatment of Alzheimer's disease. This study reveals the molecular behavior of CD synthesis. We find that research on nanozymes is now at the theoretical level, with the development of more efficient nanozymes for the treatment of diseases based on a theoretical basis. However, most of the nanozymes are designed with a material focus. When applied to disease treatment, research is rarely disease-oriented to develop a more efficient nanozyme. As an emerging cross-cutting direction, the orientation toward clinically significant needs should be fundamental to drug design. Herbzymes is a concept that aims to combine herbal medicines and nanozymes using modern technology toward clinical needs.

The CCzymes we developed using CC as a precursor material demonstrated powerful effects in the treatment of UC. Despite our progress in the application of CCzymes, however, our study still has some limitations. First, due to the complexity of precursor materials, it is difficult for us to reveal the specific molecular behavior of CCzymes synthesis. In addition, we can only reveal the antioxidant enzyme activities of CCzymes from a certain perspective. However, the surface of CDs is never clean, so our studies on CCzymes are far from enough. This is also a difficult problem in the field of CDs research. More advanced in situ or in-work characterization techniques to detect the changes that occur on the surface of carbon materials during work may advance the field.

4 | CONCLUSION

In this study, we developed CCzymes with inherent antioxidant activity from the herbal medicine CC, aiming to prevent and treat UC by leveraging free radical scavenging and anti-inflammatory mechanisms. Specifically, the oxidative polymerization process enriched the surface of the as-prepared CCzymes with precursor material from CC, resulting in a significantly enhanced antioxidant activity compared to the CC extract. Theoretical simulation calculations elucidated the mechanism underlying the free radical scavenging activity of CCzymes, demonstrating their ability to mitigate cellular oxidative damage by scavenging excessive ROS. Concurrently, CCzymes inhibited inflammation through multiple pathways, attributable to the inherited pharmacological activity of flavonoids. This inhibition involved suppressing Kit expression, modulating the MAPK and PI3K-Akt signaling pathways, and regulating macrophage polarization, thereby reducing pro-inflammatory cytokine production. In vivo evaluation using a UC mouse model revealed that CCzymes, possessing excellent biosafety profiles, exhibited superior therapeutic efficacy compared to the CC extract in both acute and chronic UC models. Furthermore, CCzymes demonstrated specific modulation of gut microbiota and metabolites, a characteristic attributed to the pharmaceutical activity inherited from CC. In conclusion, CCzymes effectively treated UC not only through potent antioxidant activities but also through targeted anti-inflammatory effects, ultimately contributing to the restoration of the IEB. This research explores a novel approach to developing nanozymes from herbal medicine. The newly developed herbzymes display superior pharmacological activity compared to traditional nanozymes, representing a promising direction for developing innovative nanomedicines targeting specific diseases.

AUTHOR CONTRIBUTIONS

Z.D., C.L., K.F., M.Z., and Y.J. designed, conducted the experiments and wrote the manuscript. Y.Z., Y.Z., C.X., and B.G. provided relevant experimental technical support and helped with the investigations. M.Z., K.F., M.Z., and Y. J. supervised this study and revised the manuscript.

ACKNOWLEDGMENTS

This work was supported by the National Natural Science Foundation of China (82472127, 52101287, and 82300598). The Fundamental Research Funds for the Central Universities, China (No. xtr052023008), and the Young Talent Support Plan of Xi'an Jiaotong University, China (No. YX6J001). We thank Dr. Zijun Ren at the Instrument Analysis Center of Xi'an Jiaotong University for assisting with TEM analysis and Dr. Xiaofei Wang at the experimental biomedical center of Xi'an Jiaotong University for his kind assistance with the instrument operation and data analysis.

CONFLICT OF INTEREST STATEMENT

The authors declare no conflicts of interest.

DATA AVAILABILITY STATEMENT

The data that support the findings of this study are available from the corresponding author upon reasonable request.

ETHICS STATEMENT

All animal experiments were performed following the Principles of Laboratory Animal Care and Guidelines of the Laboratory Animal Care Committee of Xi'an Jiaotong University (No: 2024-151).

ORCID

Kelong Fan https://orcid.org/0000-0001-6285-1933
Mingzhen Zhang https://orcid.org/0000-0002-4686-6526
Yanyan Jiang https://orcid.org/0000-0002-7866-4689

REFERENCES

1. K. Vlantis, A. Wullaert, A. Polykratis, V. Kondylis, M. Dannappel, R. Schwarzer, P. Welz, T. Corona, H. Walczak, F. Weih, U. Klein, M. Kelliher, M. Pasparakis, *Immunity* **2016**, *44*, 553.
2. J. Lu, X. Shen, H. Li, J. Du, *Exploration* **2024**, *4*, 20230142.
3. K. Kandiah, S. Subramaniam, S. Thayalasekaran, F. J. Chedgy, G. Longcroft-Wheaton, C. Fogg, J. F. Brown, S. C. Smith, M. Iacucci, P. Bhandari, *Gut* **2021**, *70*, 1684.
4. N. Z. Borren, C. J. van der Woude, A. N. Ananthakrishnan, *Nat. Rev. Gastroenterol. Hepatol.* **2019**, *16*, 247.
5. L. Zhu, P. Gu, H. Shen, *Int. Immunopharmacol.* **2019**, *68*, 242.
6. R. Zhou, Y. Huang, C. Tian, Y. Yang, Z. Zhang, K. He, *Am. J. Chin. Med* **2023**, *51*, 2195.
7. L. Zhai, J. Peng, M. Zhuang, Y. Chang, K. Cheng, Z. Ning, T. Huang, C. Lin, H. L. X. Wong, Y. Y. Lam, H. Y. Tan, H. Xiao, Z. Bian, *Phytomedicine* **2022**, *99*, 154001.
8. Y. Dong, H. Fan, Z. Zhang, F. Jiang, M. Li, H. Zhou, W. Guo, Z. Zhang, Z. Kang, Y. Gui, Z. Shou, J. Li, R. Zhu, Y. Fu, A. Sarapultsev, H. Wang, S. Luo, G. Zhang, D. Hu, *Int. J. Biol. Sci.* **2022**, *18*, 1381.
9. L. Wang, T. Xu, S. Wu, C. Zhao, H. Huang, *Int. J. Antimicrob. Agents* **2025**, *65*, 107468.
10. Y. Yang, R. Ren, Q. Chen, Q. Zhang, J. Wu, D. Yin, *Phytomedicine* **2022**, *104*, 154322.
11. H. Cui, Y. Cai, L. Wang, B. Jia, J. Li, S. Zhao, X. Chu, J. Lin, X. Zhang, Y. Bian, P. Zhuang, *Front. Pharmacol.* **2018**, *9*, 571.
12. J. Lee, H. Liao, Q. Wang, J. Han, J.-H. Han, H. E. Shin, M. Ge, W. Park, F. Li, *Exploration* **2022**, *2*, 20210086.
13. C. Xia, S. Zhu, T. Feng, M. Yang, B. Yang, *Adv. Sci.* **2019**, *6*, 1901316.
14. J. Li, W. Fu, X. Zhang, Q. Zhang, D. Ma, Y. Wang, W. Qian, D. Zhu, *Carbon* **2023**, *208*, 208.
15. F. Gao, J. Liu, P. Gong, Y. Yang, Y. Jiang, *Chem. Eng. J.* **2023**, *462*, 142338.
16. F. Gao, J. Huang, Y. Ruan, H. Li, P. Gong, F. Wang, Q. Tang, Y. Jiang, *Angew. Chem., Int. Ed.* **2023**, *62*, 202214042.
17. Z. Deng, Y. Zhang, R. Li, Y. Zhu, C. Xu, B. Gao, W. Wang, C. Ding, B. He, X. Zhu, M. Yang, T. Liang, M. Zhang, *Adv. Funct. Mater.* **2025**, *35*, 2418683.
18. Y. Guo, L. Yang, L. Yao, C. Zhou, Y. Zhu, C. Xu, W. Wang, J. Song, M. Zhang, Z. Deng, *J. Nanobiotechnol.* **2025**, *23*, 391.
19. M. Xu, C. Ren, Y. Zhou, Z. Heger, X. Liang, V. Adam, N. Li, *Chin. Chem. Lett.* **2023**, *34*, 107585.
20. M. Li, L. Yang, Y. An, X. Tan, P. He, Y. Tan, R. Liu, J. Zheng, W. Zhang, Y. Jiang, Y. Chen, Z. Lu, G. Liu, *ACS Nano* **2025**, *19*, 17834.
21. Y. Pan, Y. Zhang, D. Sun, L. Kong, Y. Liu, D. Yu, K. Song, S. Ni, W. Jiang, J. Zhan, *Adv. Funct. Mater.* **2025**, 2509879.
22. Y. Xu, B. Wang, M. Zhang, J. Zhang, Y. Li, P. Jia, H. Zhang, L. Duan, Y. Li, Y. Li, X. Qu, S. Wang, D. Liu, W. Zhou, H. Zhao, H. Zhang, L. Chen, X. An, S. Lu, S. Zhang, *Adv. Mater.* **2022**, *34*, 2200905.
23. R. Chen, Z. Wang, T. Pang, Q. Teng, C. Li, N. Jiang, S. Zheng, R. Zhang, Y. Zheng, D. Chen, F. Yuan, *Adv. Mater.* **2023**, *35*, 2302275.
24. B. Geng, J. Hu, Y. Li, S. Feng, D. Pan, L. Feng, L. Shen, *Nat. Commun.* **2022**, *13*, 5735.
25. W. Fawaz, J. Hasian, I. Alghoraibi, *Sci. Rep.* **2023**, *13*, 18641.
26. H.-J. Li, Y. Chen, H. Wang, H. Wang, Q. Liao, S. Han, Y. Li, D. Wang, G. Li, Y. Deng, *Adv. Funct. Mater.* **2023**, *33*, 2302862.
27. Y. Wu, X. Chen, W. Wu, *Small* **2023**, *19*, 2206709.
28. M. Jagannathan, D. Dhinasekaran, P. Soundharraj, S. Rajendran, D.-V. N. Vo, A. Prakasarao, S. Ganesan, *J. Hazard. Mater.* **2021**, *416*, 125091.
29. D. Li, D. Han, S.-N. Qu, L. Liu, P.-T. Jing, D. Zhou, W.-Y. Ji, X.-Y. Wang, T.-F. Zhang, D.-Z. Shen, *Light: Sci. Appl.* **2016**, *5*, e16120.
30. N. S. K. Gowthaman, B. Sinduja, R. Karthikeyan, K. Rubini, S. Abraham John, *Biosens. Bioelectron.* **2017**, *94*, 30.
31. D. Wang, X. Song, P. Li, X. J. Gao, X. Gao, *J. Mater. Chem. B* **2020**, *8*, 9028.
32. W. Gao, J. He, L. Chen, X. Meng, Y. Ma, L. Cheng, K. Tu, X. Gao, C. Liu, M. Zhang, K. Fan, D.-W. Pang, X. Yan, *Nat. Commun.* **2023**, *14*, 160.
33. H. Sun, A. Zhao, N. Gao, K. Li, J. Ren, X. Qu, *Angew. Chem., Int. Ed.* **2015**, *54*, 7176.
34. J. Huang, F. Gao, Q. Liu, P. Gong, H. Li, Y. Jiang, *Small* **2024**, *20*, 2309637.
35. S. Srikanth, V. Aparna, S. R. Balakrishnan, *Gut* **2007**, *56*, 1543.
36. Ł. Kopiasz, K. Dziendzikowska, M. Gajewska, J. Wilczak, J. Harasym, E. Żyła, D. Kamola, M. Oczkowski, T. Królikowski, J. Gromadzka-Ostrowska, *Antioxidants* **2020**, *9*, 375.
37. L. Li, J. Tan, Y. Miao, P. Lei, Q. Zhang, *Cell. Mol. Neurobiol.* **2015**, *35*, 615.
38. J. Van den Bossche, J. Baardman, N. A. Otto, S. van der Velden, A. E. Neele, S. M. van den Berg, R. Luque-Martin, H. J. Chen, M. C. Boshuizen, M. Ahmed, M. A. Hoeksema, A. F. de Vos, M. P. de Winther, *Cell Rep.* **2016**, *17*, 684.
39. Y. Ma, J. Zhao, L. Cheng, C. Li, X. Yan, Z. Deng, Y. Zhang, J. Liang, C. Liu, M. Zhang, *Carbon* **2023**, *204*, 526.
40. T. Regad, *Cancers* **2015**, *7*, 1758.
41. J. Copeland, M. Simoes-Costa, *P. Natl. Acad. Sci. USA* **2020**, *117*, 33305.
42. T. Fischer, O. Hartmann, M. Reissland, C. Prieto-Garcia, K. Klann, N. Pahor, C. Schülein-Völk, A. Baluapuri, B. Polat, A. Abazari, E. Gerhard-Hartmann, H. G. Kopp, F. Essmann, M. Rosenfeldt, C. Münch, M. Flentje, M. E. Diefenbacher, *Cell Biosci.* **2022**, *12*, 50.

43. H. Cheng, P. Liu, C. Ohlson, E. Xu, L. Symonds, A. Isabella, W. J. Muller, N. U. Lin, I. E. Krop, T. M. Roberts, E. P. Winer, C. L. Arteaga, J. J. Zhao, *Oncogene* **2016**, *35*, 2961.
44. F. O. Martinez, S. Gordon, M. Locati, A. Mantovani, *J. Immunol.* **2006**, *177*, 7303.
45. T. Wang, D. Pan, Z. Zhou, Y. You, C. Jiang, X. Zhao, X. Lin, *PLoS Pathog.* **2016**, *12*, e1005662.
46. C. H. Fong, M. Bebien, A. Didierlaurent, R. Nebauer, T. Hussell, D. Broide, M. Karin, T. Lawrence, *J. Exp. Med.* **2008**, *205*, 1269.
47. X. Yan, C. Yang, M. Yang, Y. Ma, Y. Zhang, Y. Zhang, C. Liu, Q. Xu, K. Tu, M. Zhang, *J. Nanobiotechnol.* **2022**, *20*, 99.
48. L. Pan, H. Yu, J. Fu, J. Hu, H. Xu, Z. Zhang, M. Bu, X. Yang, H. Zhang, J. Lu, J. Jiang, Y. Wang, *Acta Pharm. Sin. B* **2023**, *13*, 1537.
49. I. Sulaiman, B. G. Wu, Y. Li, J. C. Tsay, M. Sauthoff, A. S. Scott, K. Ji, S. B. Koralov, M. Weiden, J. C. Clemente, D. Jones, Y. J. Huang, K. A. Stringer, L. Zhang, A. Geber, S. Banakis, L. Tipton, E. Ghedin, L. N. Segal, *Eur. Respir. J.* **2021**, *58*, 2003434.
50. X. Tang, W. Wang, G. Hong, C. Duan, S. Zhu, Y. Tian, C. Han, W. Qian, R. Lin, X. Hou, *J. Biomed. Sci.* **2021**, *28*, 20.
51. G. Li, X. Guo, J. Luo, J. Guo, S. Xiao, X. Yang, X. Shi, J. Xiang, J. Yang, T. Ma, C. Lu, L. Zheng, J. Zhao, J. Zhong, *Nano Today* **2024**, *56*, 102250.
52. J. Yang, R. Zhang, H. Zhao, H. Qi, J. Li, J.-F. Li, X. Zhou, A. Wang, K. Fan, X. Yan, T. Zhang, *Exploration* **2022**, *2*, 20210267.
53. T. Ye, C. Chen, D. Wang, C. Huang, Z. Yan, Y. Chen, X. Jin, X. Wang, X. Ding, C. Shen, *Nat. Commun.* **2024**, *15*, 1682.
54. K. Fan, J. Xi, L. Fan, P. Wang, C. Zhu, Y. Tang, X. Xu, M. Liang, B. Jiang, X. Yan, L. Gao, *Nat. Commun.* **2018**, *9*, 1440.
55. C. Wu, D. Xu, M. Ge, J. Luo, L. Chen, Z. Chen, Y. You, Y.-x. Zhu, H. Lin, J. Shi, *Nano Today* **2022**, *46*, 101574.
56. W. H. Gao, J. Y. He, L. Chen, X. Q. Meng, Y. N. Ma, L. L. Cheng, K. S. Tu, X. F. Gao, C. Liu, M. Z. Zhang, K. L. Fan, D. W. Pang, X. Y. Yan, *Nat. Commun.* **2023**, *14*, 160.
57. P. Yang, Q. Huang, J. Zhang, Y. Li, H. Gao, Z. Gu, *Adv. Mater.* **2023**, *36*, 2308393.

SUPPORTING INFORMATION

Additional supporting information can be found online in the Supporting Information section at the end of this article.

How to cite this article: Z. Deng, C. Li, Y. Zhang, Y. Zhu, C. Xu, B. Gao, M. Zhang, M. . H. Stenzel, K. Fan, M. Zhang, Y. Jiang, *BMEMat* **2026**, *4*, e70031. https://doi.org/10.1002/bmm2.70031